Removal of Cationic and Anionic Dyes from Textile Waste Effluent using a Magnetic Nanocomposite made of Activated Carbon and Magnesium Doped Bismuth Ferrite

Sabrine Saad[1]·. Assia Hassen[1], Amel Ben Slimane[1]

1. Laboratory of Materials Applications in Environment, Water and Energy, Faculty of Sciences, University of Gafsa, Tunisia.

Corresponding authors:

Amel Ben Slimane (amelbenslimane71@yahoo.fr); https://orcid.org/0000-0001-8195-6423

Sabrine Saad (sabrine.saad2017@gmail.com); https://orcid.org/0009-0003-5646-6328

Abstract

The ($BiMgFeO_4$/activated carbon) composite has been developed deploying glycine as fuel in a self-combustion process. It was employed to remove methyl green (MG), a cationic dye, and methyl orange (MO), an anionic dye, from aqueous solutions. It was characterized by specific surface area measurement (BET), scanning electron microscopy (SEM), Fourier transform infrared spectroscopy (FTIR), and X-ray diffraction (XRD). FTIR spectra showed three bands located around 548.18 cm^{-1}, 973. cm^{-1}, and 1577.01 cm^{-1} attributed to the stretching vibrations of Bi-O, Fe-O, Mg-O, and O-H, respectively. The SEM images revealed a highly porous and irregular structure beneficial for the effective diffusion of dye molecules. The sample contains a notable proportion of holes with different sizes of pores. The microcavities observed on the adsorbent surface were conducive to good diffusion of the dye molecules. The composite's mesoporous structure was deduced by BET analysis, which allowed us to determine the material's specific surface area of 20.289 m^2/g and its pore diameter of 7.54 nm. X-ray diffraction showed peaks attributed to Fe_3O_4, MgO, and Bi_2O_3 (confirming the presence of $BiMgFeO_4$ ferrite) and other peaks attributed to dehydrated hemicellulose and carbon/graphite (confirming the use of activated carbon). The various experimental parameters affecting the performance of this reaction, such as temperature, contact time, initial dye concentration, and adsorbent mass, were studied. The composite's pH zero charge point (pH_{PZC}) was found to be 8.77. The equilibrium isotherms were described using the Freundlich and Langmuir adsorption models. The equilibrium time was a function of the starting dye concentration in the adsorption tests. Adsorption equilibrium for ($BiMgFeO_4$/activated carbon) was formed after 120 min, according to adsorption kinetic analysis. Moreover, the results revealed that pseudo-second-order kinetics could correctly characterize the adsorption of MO and MG on the composite. Adsorption isotherms confirmed that the adsorption process of both dyes onto the ($BiMgFeO_4$/activated carbon) composite was successful. The Langmuir model appears to be best suited to the adsorption of MO and MG on the($BiMgFeO_4$/activated carbon), with a maximum adsorption capacity of 196.078 $mg.g^{-1}$ and 192.307

mg.g^{-1} respectively, at 298 K. The adsorption of the two dyes was spontaneous and exothermic, in line with the thermodynamic parameters associated with the sorbent/adsorbate system. The determination of the isosteric heat of adsorption revealed that physisorption takes place with weak intermolecular interactions between the two dyes and the composite surface.

Keywords: Magnetic nanoferrite • Activated carbon• Composite • Adsorption • Methyl orange • Methyl green

Abbreviations

$BiMgFeO_4$: Mg-doped bismuth ferrite

$BiMgFeO_4$/activated carbon: Mg-doped bismuth ferrite- activated carbon

MO: Methyl orange

MG: Methyl green

FTIR: Fourier-transform infrared

SEM: Scanning electron microscopy

XRD: X-ray diffraction

SBET: Brunauer–Emmett–Teller surface area

pH_{PZC}: The pH of point of zero charge

1 Introduction

The manufacture of colorants and their application in numerous modern industrial sectors are continuously expanding. They find applications in the food, paper, pharmaceutical, textile, and cosmetics sectors. However, dyes are a major hazard to the ecosystems and the health of organisms because they accumulate in industrial wastes [1-3]. Numerous research teams have been focused on developing efficient and fast methods of treating contaminated water in the past few decades. Among the wastewater treatment methods are adsorption, coagulation-flocculation, membrane separation, chemical oxidation, and biological treatment [4,5].

Adsorption proved to be particularly interesting and successful in treating organic dye-contaminated water. Studies have been conducted on a variety of synthetic and natural adsorbents; the most well-known is activated carbon, whose preparation costs are still rather high [6–8].

However, because of their remarkable ability to adsorb large amounts of organic and inorganic pollutants present in aqueous solutions, and since they can be recycled to remove more dyes, magnetic materials—and in particular, magnetic nanocomposites—have attracted much interest [9,10]. In recent years, several types of ferrite have been studied for their interesting magnetic, electrical, and

optical properties and have seen a variety of applications. Doped ferrites have been specifically applied to antibacterial activity, dye and heavy metal removal, and photodegradation [3,11].

It is commonly known that activated carbon plays a crucial role in the adsorption of pollutants. A material with a remarkable porous structure, activated carbon is derived from carbon-based materials such as wood or coconut shells. Its main applications include drinking water purification, air decontamination, and wastewater treatment [4]. It is suggested to use activated carbon to eliminate several kinds of contaminants, including chemicals, volatile organic compounds, heavy metals, and other undesired materials. The ability to reuse activated carbon over extended periods is a significant benefit. This regeneration process, often achieved by heating and releasing absorbed contaminants, turns activated carbon into recyclable material [12,13]. Due to its remarkable capacity to absorb a wide range of pollutants and thereby aid in the purification of our key resources, activated carbon is playing an increasingly important role in maintaining the purity of the environment and human health [14,15].

To treat water contaminated by two dyes, one cationic dye, Methyl Green (MG), and the other anionic dye, Methyl Orange (MO) [16,17], we have suggested creating a novel composite ($BiMgFeO_4$/Activated Carbon) from a new $BiMgFeO_4$-doped nanoferrite [18,19,11] Both of these dyes are widely used colors in the textile industry. So, they are among the most common organic pollutants found in wastewater.

The $BiMgFeO_4$/activated carbon composite was produced by a self-combustion method developed from the sol-gel process, using glycine as fuel [20]. This composite was characterized by scanning electron microscopy (SEM), Fourier transform infrared (FTIR), X-ray diffraction (XRD), and measuring its specific surface area using the BET method [21-23]. We investigated the effects of adsorbent dose, contact time, initial pH, and temperature on the adsorption of organic dyes in a discontinuous system [24]. We have also performed a thermodynamic and kinetic study and applied some models of adsorption isotherms, such as the Freundlich and Langmuir models [25-28].

2 Materials and Methods

2.1. Chemicals Materials

Ferric nitrate nonahydrate ($Fe(NO_3)_3.9H_2O$), Magnesium nitrate hexahydrate Magnesium nitrate $Mg(NO_3)_2.6H_2O$, Bismuth nitrate pentahydrate $Bi(NO_3)_3.5H_2O$, the Glycine $C_2H_5NO_2$. Sodium hydroxide (BioXtra, ≥98%) and hydrochloric acid (HCl, ACS reagent, 37%) were provided by Sigma-Aldrich , Methyl Orange ($C_{14}H_{14}N_3NaO_3S$) and Methyl Green were supplied by Scharlau.

For the activated carbon, the raw material used originates from the Oméga Tunisie essential oil extraction company, located in the Sidi Bouzid region. These seeds are the final by-product of the prickly pear essential oil extraction process [29-31].

2.2. Preparation of Activated carbon

2.2.1. Raw materia

In the search for new precursors, prickly pear seeds were included in this study,. Prickly pears are grown all around the Mediterranean region; due to its warm climate conducive to the development of the prickly pear, but also to its physico-chemical characteristics. Tunisia has been classified as one of the most productive countries for this fruit, and used in many food and cosmetic applications [30, 31]. Prickly pear seed oil cake has been produced in large quantities as a by-product of the Prickly pear seed oil extraction industry. Consequently, the preparation of activated carbons with this raw material is an interesting approach in order to valorize this raw material [32]. The raw material used originates from the Oméga Tunisie essential oil extraction company, located in the Sidi Bouzid region.

2.2.2. Activated carbon preparation process

The following figure (**Fig. 1**) illustrates the process for converting the biomass under consideration into activated carbon.

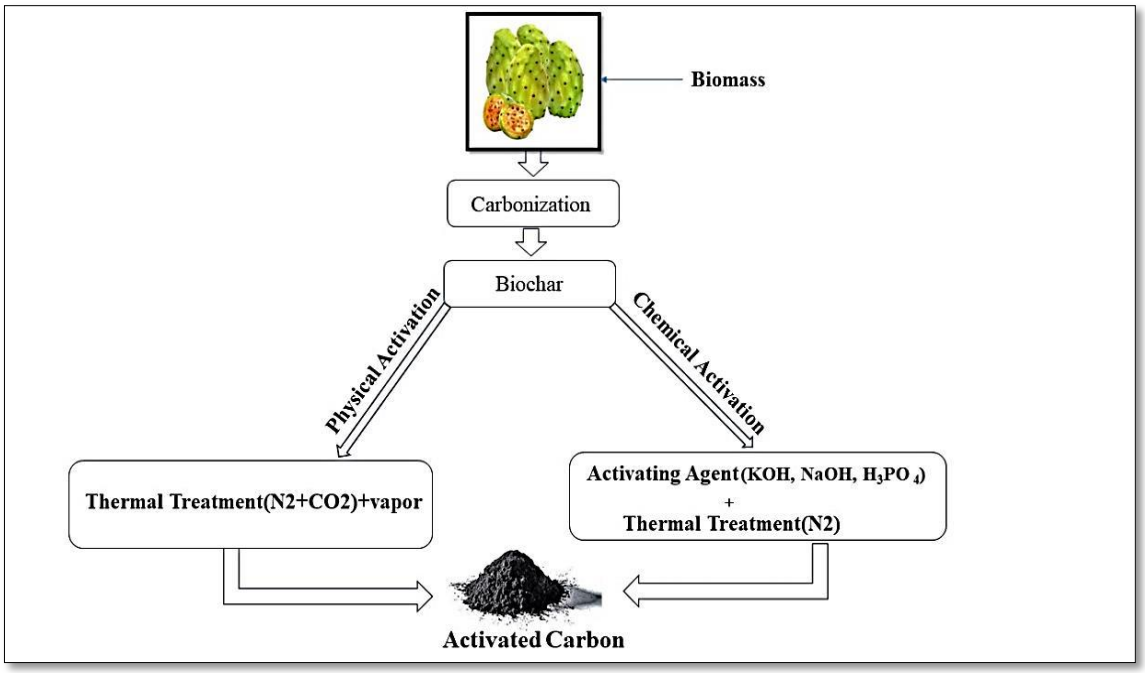

Fig. 1 Process for preparing activated carbon from biomass

2.3 Preparation of Nanomaterials

2.3.1 The General Strategy of the Work

The composite was produced by the process of self-combustion. Subsequently, we explained that it possesses the ability to chelate metals by creating a highly stable and soluble complex while maintaining solvent volume. A more detailed explanation is provided in Sect. **2.3.2.**
Figure 2 shows the entire preparation and application process of an adsorbent.

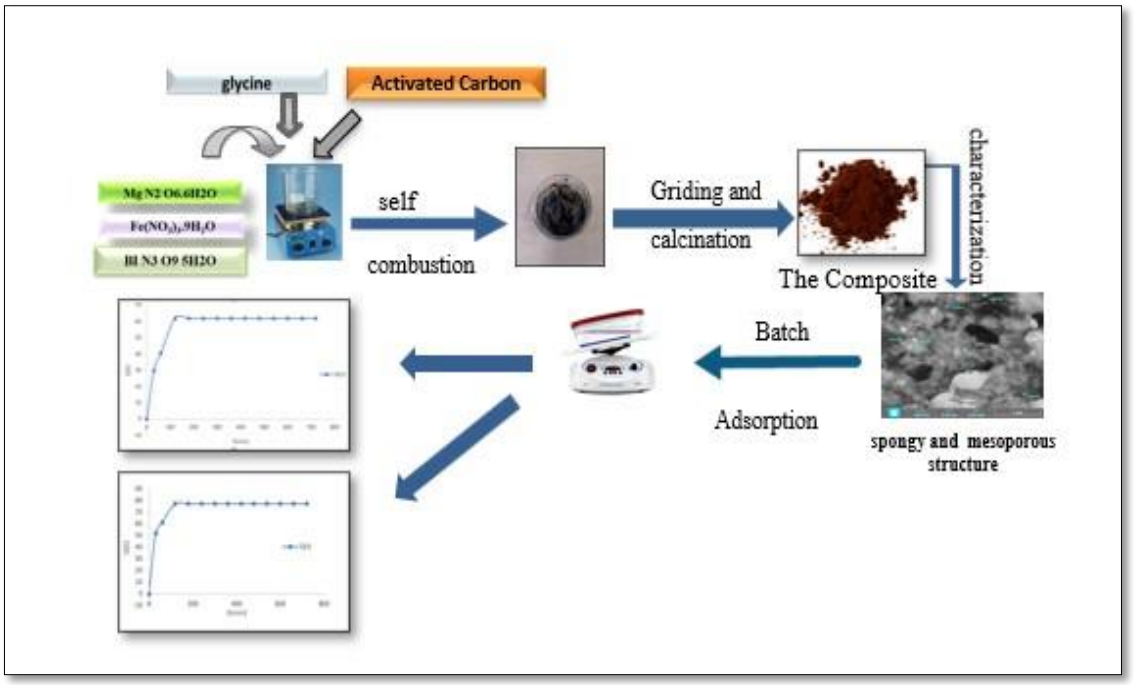

Fig. 2 The general strategy of preparation of $BiMgFeO_4$/Activated carbon Nanoparticles

2.3.2 Preparation of the $BiMgFeO_4$/Activated carbon Composite

$BiMgFeO_4$/Activated carbon composite was synthesized using the same process for the production of Mg-doped bismuth ferrite powder $BiMgFeO_4$ nanoferrite by the self-combustion method [33]. However, Activated carbon was inserted before the addition of the combustible agent. The raw materials used are iron (III) nitrate $Fe(NO_3)_3.9H_2O$, magnesium (II) nitrate $Mg(NO_3)_2.6H_2O$, bismuth(III) nitrate $Bi(NO_3)_3.5H_2O$, Activated carbon and glycine $C_2H_5NO_2$. The chemicals were dissolved in distilled water in accordance with a calculated stoichiometric ratio, and all component molar ratios were set to one (except glycine). The combustible agent (Glycine) was introduced after a few minutes respecting the following condition:

$$n\ \text{glycine} = nFe^{3+} + nMg^{2+} + nBi^{3+}$$

where n is the mole number.

An equimolar concentration of bismuth nitrate pentahydrate ($Bi(NO_3)_3.5H_2O$),ferric nitrate nonahydrate ($Fe(NO_3)_3.9H_2O$ and magnesium nitrate hexahydrate ($Mg(NO_3)_2.6H_2O$) were dissolved independently in 50 mL of distilled water. Bismuth nitrate pentahydrate $Bi(NO_3)_3.5H_2O$ was added after ferric nitrate nonahydrate $Fe(NO_3)_3.9H_2O$ and magnesium nitrate hexahydrate $Mg(NO_3)_2.6H_2O$ were combined at 80–90 °C while being stirred by heat until a homogenous mixture was formed. A little while later, the combustible agent (glycine) was added after the activated carbon (Fig.2).

The obtained homogeneous solution was mixed under thermal stirring 80-180°C. Stirring continuously for 3 hours, then the solution was evaporated in order to obtain a dry gel. This last was then forced by self-ignition by rapid heating. The rapid evaluation of a large volume of gas is accompanied by a significant loss of mass during combustion, leading to the formation of numerous foams and sparks, resulting in a bulky and fluffy product in the container. The obtained fine powder was ground with a mortar and pestle to obtain nanoparticles. Finally, it was kept in an oven for 3 hours at a temperature in the area of 80°C-180°C to improve its crystallinity and remove residual organic matter.

2.4. Characterizations of the Nanoparticles

The synthesized composite was subjected to FTIR measurement at room temperature in a range of 400 to 4000 cm^{-1} using KBr pellets solid (10% solid) in a Shimadzu 8400-S spectrometer.

Using Meso400A-01-Analysis equipment, and static volumetric method, N_2 adsorption-desorption measures were performed at 77.35 K to determine the synthesized material's Brunauer–Emmett–Teller (SBET) specific surface area and pore structure parameters. The sample (0.1 g) was degassed for eight hours at 300°C before measurement.

We recorded powder diffractograms using a Powder X-ray diffraction (PXRD) D8 Advance Bruker two-circle diffractometer equipped with a Lynx eye detector. The θ-2θ scan utilized the dichromatic copper radiation (λ CuK α_1/α_2). These were the wavelengths: $\lambda_{K\alpha2}$ = 0.154 439 nm and $\lambda_{K\alpha1}$ = 0.154 060 nm. Complete diffraction power of 30 mA / 40 kV. Scanning: drive axis: θ-2θ, scan range: 10.0000 - 80.0000 (deg), scan mode: Continuous Scan, scan speed: 2.0000 (deg/min), sampling pitch: 0.2000 (deg), preset time: 6.00 (sec)

The morphology of the prepared material was assessed using scanning electron microscopy (SEM) micrographs obtained with a ZEISS-ULTRA55 SEM microscope that is completely controlled from a computer workstation. An accelerating voltage of 20 kV was applied to the zirconated tungsten filament.

The pH of the point of zero charge (pH_{PZC}) was determined using the pH drift method [34]. Aqueous solutions with various pH values between 2 and 12 and NaCl (0.1 M) were created by adding sodium hydroxide and hydrochloric acid. Then, the NaCl solutions were mixed with 0.15 g of nano

ferrite. When the pH was adjusted to a value between 2 and 12, the suspension reached equilibrium after 2.5 hours of agitation. A correlation was established between the initial pH and the final pH measured. The nanomaterial's zero charge point (PZC) is the pH value at which the pH (final) = pH (initial) line intersects. However, each of these various pH tests was carried out simultaneously.

2.5 Batch Adsorption

2.5.1 Analytical Method

After the adsorption tests, the concentration of both dyes was measured using a Beckman UV/Vis DU 800 Spectrophotometer, with λ_{max} = 465 nm for Methy Orange and 632 nm for Methyl Green as the maximum wavelengths. Eq. (1) was utilized to determine the equilibrium adsorption capacity Q (mg. g^{-1}):

$$Q = \frac{(C_0 - C_e)V}{m} \quad (1)$$

With V (L) representing the volume of the solution, m (g) as the mass of the composite, Ce (mg. L^{-1}) as the equilibrium concentration of the contaminant under study, and C_0 being its initial concentration.

2.5.2 Effect of Initial pH, Adsorbent Dose and Temperature

To determine the impacts of temperature, initial pH, and adsorbent dose, batch mode pollutant adsorption tests were conducted. In order to assess the impact of initial pH, we have performed studies at room temperature using 10 mL of dye solution (50 mg. L^{-1}). After adding a fixed dose of 10 mg of adsorbent, a pH meter was used to adjust the pH from 2 to 12 by adding HCl or NaOH solutions (0.1 mol. L^{-1}). In a water bath shaker under temperature control at 60 rpm, the solutions were shaken for 720 minutes. After filtering the samples, the concentration was measured.

We conducted experiments with adsorbent dosages ranging from 5 to 150 mg to find the most effective one. The tests were performed using the same methodology and conditions as previously mentioned.

In order to evaluate the influence of temperature on the adsorption process of the composite, we mixed 50 mg of the composite under study with 100 mL of dye solutions (C = 50 mg L^{-1}), and we observed the reaction at various temperatures (2, 7, 15, 25, 40, 60, and 75 °C).

2.5.3 Adsorption Kinetic Studies

To assess the effect of contact time on adsorption, the subsequent processes were used: At room temperature (25 °C) and for the required contact period (which can vary from 0 to 720 minutes), 50 mg of adsorbent was mixed with 100 mL of the investigated dye solution (50 mg. L^{-1}).

2.5.4 Adsorption Isotherms

The initial dye concentration (20-200 $mg.L^{-1}$) was varied for 720 minutes to conduct the experiments. A mass of 50 mg of adsorbent was used in each test. Using Langmuir's Equation, Eq. (2) [35], and Freundlich Equation, Eq. (3) [36] the experimental points were analyzed:

$$Q_e = \frac{K_L C_e}{1+K_L C_e} \quad (2)$$

$$Q_e = K_F C_e^{\frac{1}{n}} \quad (3)$$

Ce is the concentration at equilibrium; Qe is the amount adsorbed; K_F is the Freundlich constant (heterogeneity factor); and 1/n is the Freundlich coefficient. K_L is the Langmuir equilibrium constant linked to the adsorption affinity. K_F corresponds to the sorption capacity, and n to the sorption affinity.

3. Results and Discussions

3.1 Characterization of the $BiMgFeO_4$/Activated carbon Composite with Infrared Spectrum

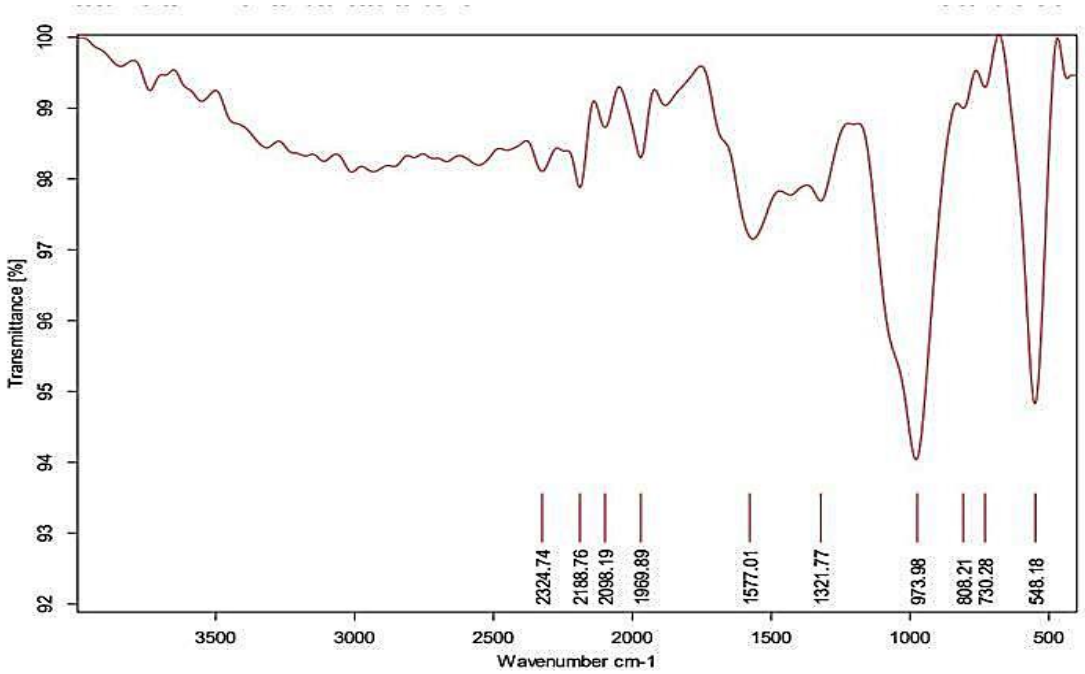

Fig. 3 FTIR spectra of $BiMgFeO_4$/Activated carbon composite

The study of the $BiMgFeO_4$/Activated carbon Composite's infrared spectra (Fig. 3) revealed a large absorption band ranging from 2500 to 3500 cm^{-1}, which was associated with the internal OH groups' elongation vibrations. In addition to the stretching vibrations of the adsorbed water, the band at 1577 cm^{-1} could also be attributed to the valence vibrations of the OH group of the constituent water. Moreover, the vibrations of the nitrate generated from the iron nitrate nonahydrate, a component ofthe

composite, are responsible for the peak at 1321.77 cm^{-1}. In general, the infrared spectrum of spinel ferrites exhibited characteristic bands associated with intrinsic vibrations of the oxygen bonds with metal cations on the two subarrays [37,38]. The metal–oxygen bands were found in the 400–1000 cm^{-1} range. The Fe–O stretching vibration, which matched the first band on the spectrum, was detected at about 419 cm^{-1}. The elongation of the Mg-O bond was responsible for the second band, located at 548.18 cm^{-1}, while the Bi-O stretching vibration was responsible for the third band, located at 730.28 cm^{-1} [39, 40]. The significant band at 973.98 cm^{-1} is commonly described in oxidized carbons and has been associated with C-O elongation in acid groups, alcohols, phenols, ethers, and/or ester groups [41], found in activated carbons. The spectrum's weakly intense band at around 1450 cm^{-1} can be assigned to the methyl group (CH in CH_3), the deformation (bending) band of O-H in activated carbon, and/or the deformation (bending) vibrations (δ) of CH_2. The aromatic C=C bonds responsible for the adsorption peaks between 2000 and 2300 cm^{-1} in the IR spectrum of the $BiMgFeO_4$ /activated carbon composite derive from the benzene-rich aromatic structure of activated carbon derived from prickly pear (lignin). Activated carbon obtained from prickly pear contains an abundance of aromatic organic molecules which give rise to characteristic adsorption bands in this region of the infrared spectrum. These peaks are due to the vibrations of the valence of the C=C bonds of the aromatic rings present in the structure of the activated carbon [42].

3.2 Characterization of the $BiMgFeO_4$/activated carbon composite with Scanning Electron Microscope (SEM) Micrographs

Images from a scanning electron microscope of the $BiMgFeO_4$/Activated carbon composite (Fig. 4a-f) at different magnifications are shown in Figure 4.

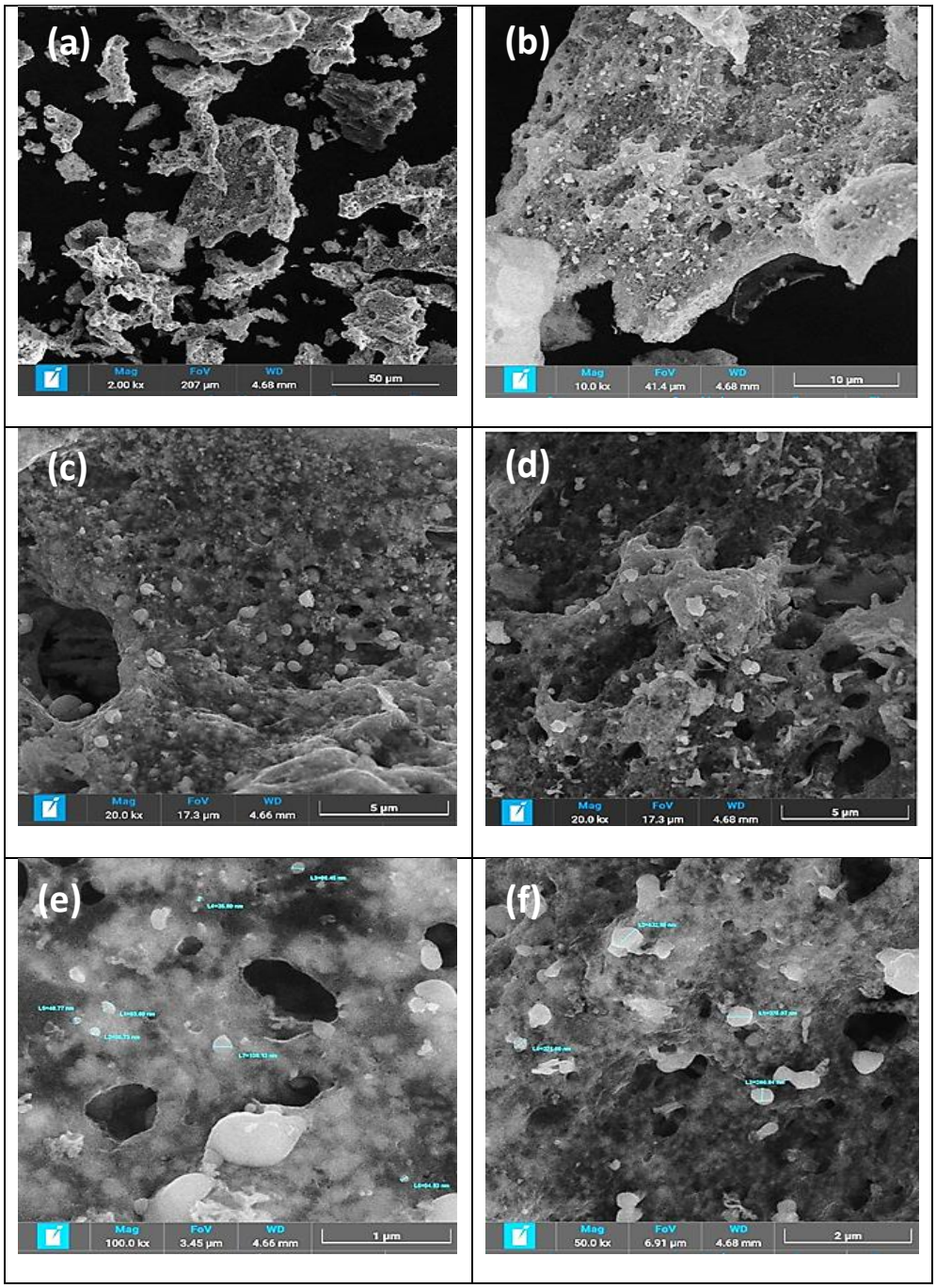

Fig. 4 SEM images of $BiMgFeO_4$/ Activated Carbon composite (**a- f**) at different magnifications

At high magnifications, nodular and non-homogeneous particles of different sizes were visible on the surface of the composite (Fig. 4c-f). On the other hand, SEM images showed an irregular and very porous structure advantageous for good diffusion of dye molecules, with a significant fraction of holes and varied pore sizes present in the sample (Fig. 4d). The emission of several gases (NO, NO_2, CO, NH_3, and H_2O) during combustion process may often be deployed to explain the voids and a highly porous structure [43, 44].

An important spongy structure was observed in the $BiMgFeO_4$/Activated Carbon composite (Fig. 4a, b), which was specifically caused by the effect of the glycine utilized as the combustion agent. The voids, which related to the release of a significant amount of gases during the combustion process, were identified as the source of the different-sized pores seen in the sample. Since the ejection of associated gas resulted in a highly porous structure with non-homogeneous and agglomerated particles. The porosity that resulted was an essential factor in the development of adsorption.

The morphological structure of the ferrite-derived composite's surface and the amount and size of its pores and cavities have all been changed by the addition of activated carbon during its production. The resultant composite revealed surface enrichment due to enhanced porosity and improved spongy structure and heterogeneity of the adsorbent. This occurrence enhanced the composite's capacity to adsorb dyes.

3.3 Characterization of the $BiMgFeO_4$/Activated carbon composite with X-ray Diffraction (XRD)

Figure 5 displays the X-ray diffractogram of the $BiMgFeO_4$/activated carbon composite

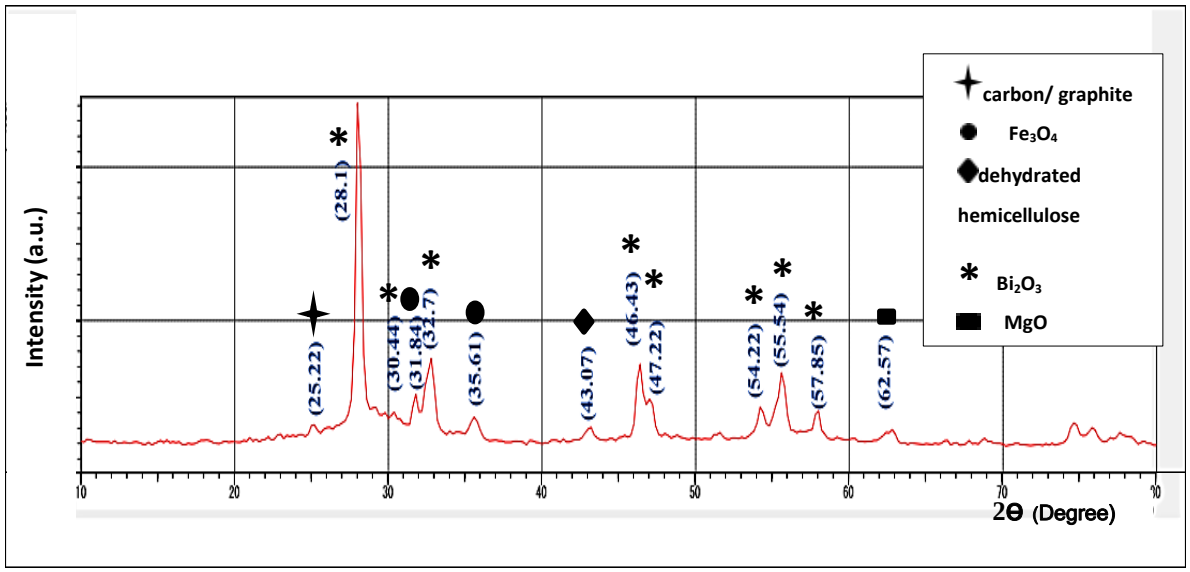

Fig.5 XRD diffractogram of the $BiMgFeO_4$/Activated carbon composite

The X-ray diffraction (XRD) analysis of the $BiMgFeO_4$/activated carbon composite sample shown in Figure 5 revealed the presence of the following crystallized phases:

- Bismuth oxide (Bi_2O_3): in various positions, Bi_2O_3 appears to be the most common element in this species, seen from different angles thanks to multiple corresponding peaks. Its existence is confirmed by peaks at 28.099°, 30.4428°, 32.7°, 46.43°, 47.22°, 54.22°, 55.54° and 57.85°. The frequency of these peaks indicates the high crystallinity of this compound in the sample.

- Fe_3O_4 (Magnetite): Peaks are also observed at 31.84° and 35.61°, although the presence of magnetite is less significant than that of Bi_2O_3. Despite the decrease in abundance, these peaks indicate a significant presence of Fe_3O_4 in the sample.
- Carbon/Graphite: Carbon or graphite is present in the peak at 25.21°, but appears to be less abundant than Bi_2O_3 or magnetite, as the peak is single and less intense.
- Magnesium oxide (MgO): Although less dominant than Bi_2O_3, MgO is also present. Its peak at 62.57° indicates that it is present in the sample.
- Dehydrated hemicellulose: Although less obvious, the presence of dehydrated hemicellulose was also detected at the peak at 43.07°, suggesting a low presence of dehydrated hemicellulose in the sample relative to the other elements.

3.4 Measurement of the Specific Surface Area of the Composite by BET Analysis

The specific surface area and the distribution and pore size were determined from adsorption–desorption isotherms of liquid nitrogen at – 195.8° C (77.35 K) [45]. Because of the limitations in N_2 adsorption, this approach can only assess the material's external surface [46]. The composite results are provided below (Fig. 6).

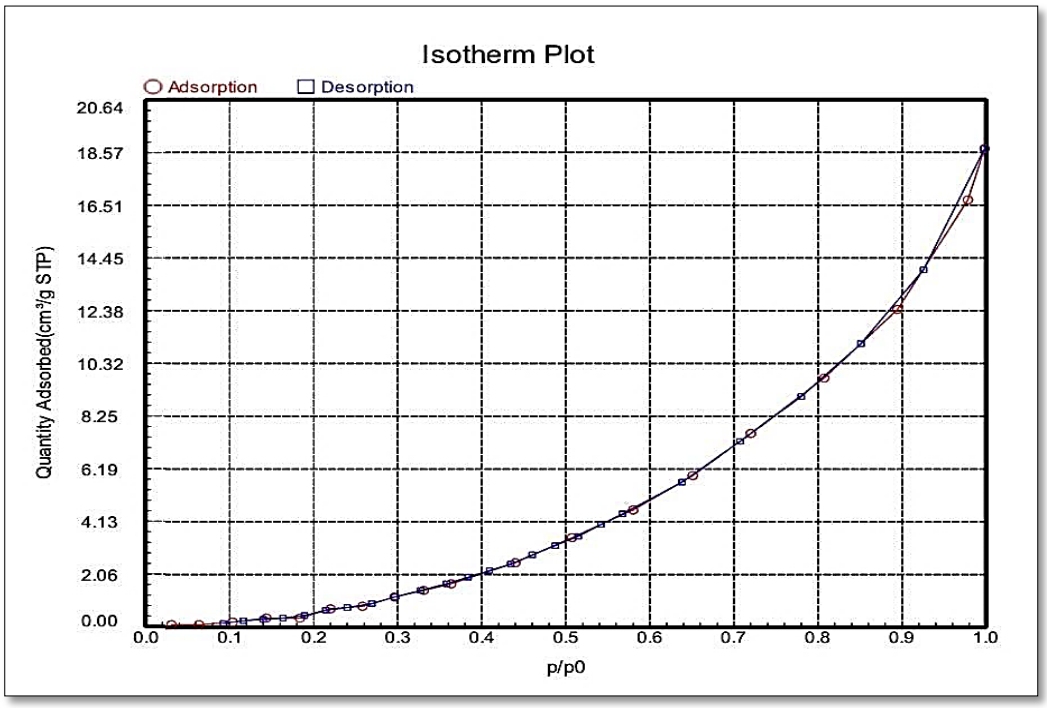

Fig.6 Adsorption and desorption isotherms of N2 on $BiMgFeO_4$/activated carbon composite

Figure 6 displays the analysis of nitrogen adsorption and desorption isotherms at low temperatures, and shows that, at low pressures, there is strong adsorption followed by a gradual increase in the quantity of adsorbed gas, which is quite significant for the composite. Then, at relatively high pressure, a capillary condensation phenomenon is observed, distinguished during desorption by the

presence of a type H3 hysteresis loop, which is quite large for the composite. suggested that the isotherm plot recorded with $BiMgFeO_4$/ Activated Carbon composite belongs to the type III adsorption isotherm in the classification of Brunauer, Deming and Teller (BDDT) [47]. That isotherm explains the formation of multilayer, and suggests relatively weak adsorbent-adsorbate interactions.

The volume of N_2 adsorbed by $BiMgFeO_4$/ Activated Carbon composite reached 18.76 cm^3/g at high pressure, due to the increase of the specific surface. The specific surface area calculated using the BET equation was 20.289 m^2/g for the composite. The size of the pore volume in the ($BiMgFeO_4$/ Activated Carbon) composite was 0.037 cm^3/g, and the pore diameter was 7.54 nm (Table 1). The mean volumes of the pores as well as their diameters of the powder were calculated by the method of Barrett—Joyner—Halenda BJH [48]. The composite was a mesoporous material with a surface area of 20.289 m^2/g and diameters of the pores ranged from 2 to 50 nm. This mesoporous structure was well suited to the removal of the anionic and cationic dyes.

Adsorbent	Pore volume (cm^3/g)	Pore diameter (nm)	Specific surface area SBET (m^2/g)
$BiMgFeO_4$/ activated carbon composite	**0.037**	**7.54**	**20.289**

Table 1 Textural and morphological of the $BiMgFeO_4$/activated carbon composite

3.5 Determination of Point of Zero Charge pH (PZC) for the $BiMgFeO_4$/activated carbon composite

The point of zero charge (pH_{PZC}) is one of the most significant parameters used to characterize the variable-charge surface properties of minerals. It is related to the charge on the particle's surface and is greatly affected by the pH of the material. The concept of point of zero charge (pzc) is important for determining the behavior of colloidal materials, particularly those with sizes smaller than one micrometer. The surface and nature of the adsorbent have a significant impact on the adsorption of any type of ion at different pH levels. The pH_{PZC} of the adsorbent can be used to describe its surface charge. When the pH at the adsorbent surface is less than pH_{PZC}, there is an excess of positive charge on the surface, which allows for the adsorption of anions. Inversely, the surface charge would be negative for pH values higher than pH_{PZC}, permitting cations to be adsorbed [49]. The experimental curve illustrating final pH versus initial pH intersects with the bisector (final pH = initial pH) to identify the pH_{PZC} of the composite [50].

The pH_{PZC} of the $BiMgFeO_4$/activated carbon composite is 8.77, as depicted in Fig. 7. The surface of the adsorbent is positively charged, and anions would be adsorbed at this pH zone if the solution's pH was lower than 8.77. Excess H+ protons from the solution would protonate the adsorbent's surface

functional groups, attracting negatively charged adsorbate to the support. The following illustration shows how the hydroxyl group bonded to the metal gets protonated:

$$(\text{M-OH} + \text{H}^{+} \rightleftharpoons \text{M-OH}_2^{+}, \quad \text{where M is metal}).$$

The surface of the composite turns negative when the pH of the solution exceeds pH_{PZC} as a result of the metal's hydroxyl group deprotonation.

$$(\text{M-OH} + \text{OH}^{-} \rightleftharpoons \text{M-O}^{-} + \text{H}_2\text{O}).$$

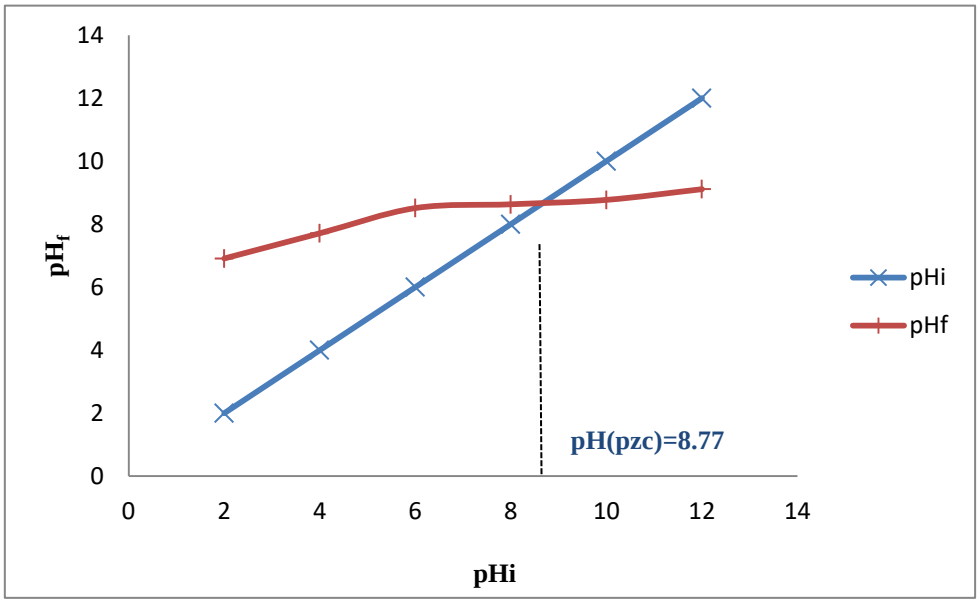

Fig. 7 Zero charge point pH_{PZC} of the $BiMgFeO_4$/activated carbon composite

3.6 Batch Adsorption Experiments

3.6.1 Effect of initial pH on the adsorption of Methyl Orange and Methyl Green

Figure 8 displays the variation of the adsorbed amount of methyl orange and methyl green on the ($BiMgFeO_4$/Activated carbon) composite versus pH.

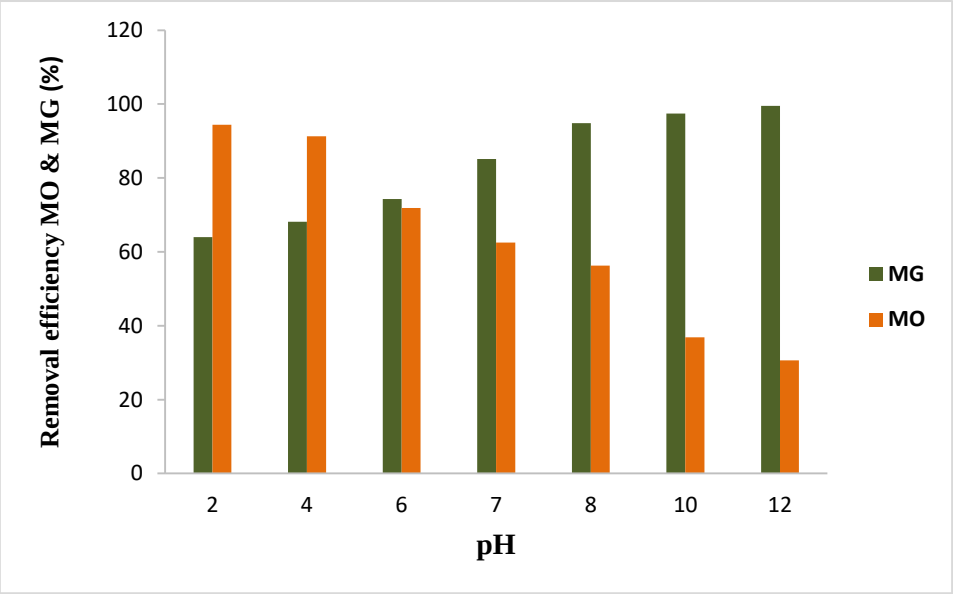

Fig. 8 pH effect on the adsorption of methyl orange and methyl green on the $BiMgFeO_4$/activated carbon composite. ([dye] = 50 mg. L^{-1}, adsorbent amount = 10 mg, time = 720 min, T = 25 °C)

The results show that the adsorption of dye onto the adsorbent was significantly affected by solution pH. It is observed that the best adsorption capacities of MO were obtained at acidic pH values (Fig.8). This could be justified based on the pH_{PZC} which is 8,77 for the obtained composite. At a pH < pH_{PZC}, the charge on the surface of the ferrite is positive, which causes a higher electrostatic attraction of the dye anions, leading to higher adsorption. At pH above pH_{PZC}, the ferrite surface charge becomes negative, so there is repulsion between the anions in the solution and the negative charge of the ferrite surface, thus, a decrease in the adsorption capacity is observed. While It was found that the amount of dye adsorbed increases from 58.86 to 99. 48% with increasing pH from 2 to 12.

Note that the pH affected the behavior of $BiMgFeO_4$/activated carbon in basic medium (pH = 9 to 12), which was observed visually, a loss of color of the solution, thus turning transparent. Therefore, the study is limited to a pH range between 2 < pH < 12. Lower adsorption capacity at lower pH (acidic medium), is mainly due to the competition between H^+ cations present in excess in the solution and cationic molecules dye for the same adsorption site onto the surface of the activated carbon.

In conclusion, acidic pH is the optimal medium to have a better adsorption of the MO anionic dye, while basic pH is the optimal medium to have a better adsorption of the MG.

3.6.2 Effect of the Adsorbent Dose on the adsorption of methyl orange and methyl green

In order to study the influence of the adsorbent dose on the adsorption of MG and MO (50 mg. L^{-1}), the mass of $BiMgFeO_4$/activated carbon composite as adsorbent was varied from 0.05 g to 1.5 g per 100 ml of sample volume (Fig. 9).

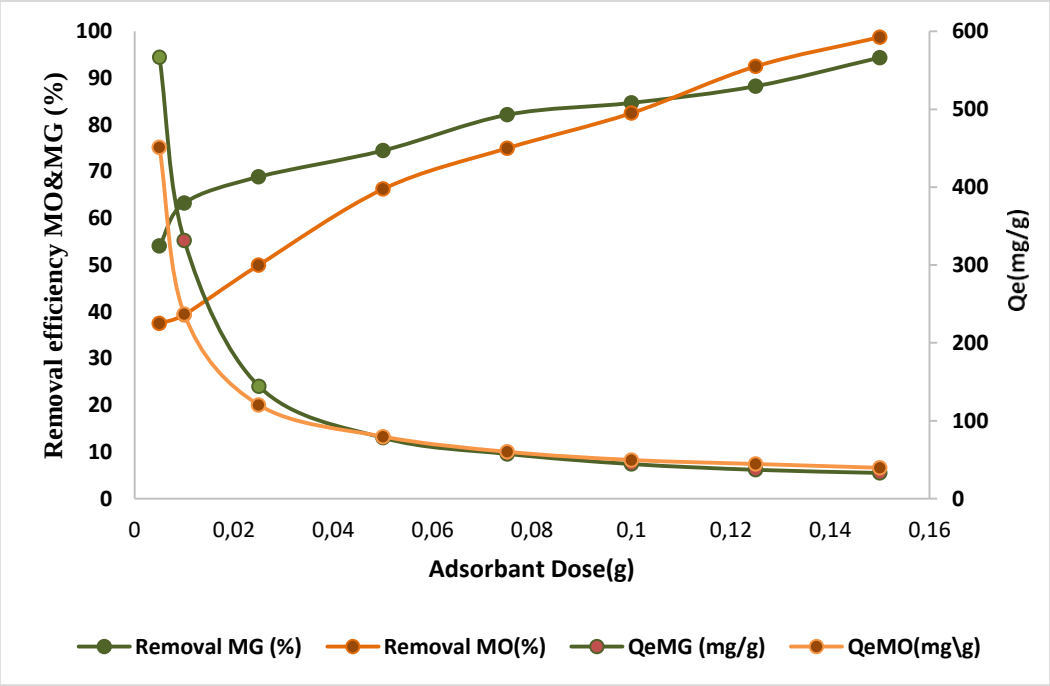

Fig. 9 The effect of the ($BiMgFeO_4$/activated carbon) composite dose on the adsorption of Methyl Green and the Methyl Orange ([Dye] = 50 $mg.L^{-1}$, time = 720 min, T = 25 °C)

The figure 9 shows that the percentage of MO removal increases (from 37.49% to 98.75 %) with increasing adsorbent mass, whereas the MO adsorption capacity decreases drastically from 451.12 to 39.59 mg/g. Because adsorption sites were entirely accessible for the polluent at low adsorbent dosage, the adsorption capacity was increased. However, at high adsorbent doses, the majority of the low-energy adsorption sites were first occupied. Consequently, the accessibility of high-energy adsorption sites significantly decreased, and adsorption capacity was reduced [51]. Moreover, the higher the adsorbent dose, the more likely collisions and agglomeration between solid particles occurred, leading to a decrease in total surface area and ferrite adsorption capacity for the polluent. Increasing the mass of the adsorbent offers an increased number of available adsorption sites and therefore increased amount of adsorbed dye [52]. While the decrease of dyes adsorption could be explained by the saturation of adsorption sites [53].

The figure above (Fig.9) demonstrates that the removal efficiency of MG increases by 54.08 % to 94.38% while the adsorption capacity of MG decreases drastically by 566.83 mg/g to 32.97. mg/g. This can be understood, as increasing the mass of the adsorbent increases the specific surface area and hence the number of adsorption sites available, leading to an increase in the amount of dye adsorbed . The decrease in the amount of MG dye adsorbed per unit mass (mg/g) could be explained by the saturation of adsorption sites.

3.6.3 Effect of the Contact Time on the adsorption of Methyl Orange and Methyl Green using $BiMgFeO_4$/ activated carbon composite

The MO and MG discoloration test by adsorption on ($BiMgFeO_4$-Activated carbon) composite (Fig.10) was performed by monitoring the contact time of the adsorption equilibrium, where a saturated state of the substrate is established. It is considered the most critical parameter in the development of an economical wastewater treatment system [40]. Thus, the identification of contact time enables adsorption isotherms to be established. In fact, the contact time is fundamental in determining the maximum adsorption quantity. The adsorption capacity or removal rate can be calculated from Eq. (4)

$$\%\ \boldsymbol{Removal} = \frac{C_0 - C_t}{C_0} \times 100 \qquad (4)$$

With C_0: initial concentration and C_t: concentration at time t.

The equilibrium studies were performed at predefined time intervals ranging from 30 to 720 min and with different adsorbent masses (10, 50, and 100 mg) (Fig.11) to determine the optimal adsorption time.

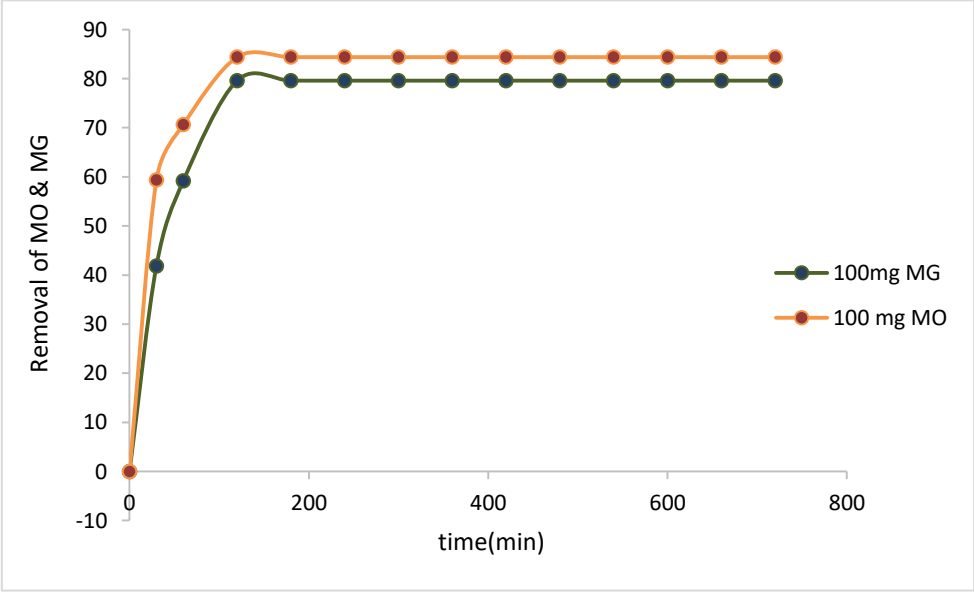

Fig.10 The effect of the contact time on the absorption of methyl orange and methyl green by $BiMgFeO_4$/activated carbon) composite

As shown in Fig.10, the adsorption of MO and MG by the composite increases steadily with time and then reaches adsorption equilibrium with percentages of 79.59% and 84.87% for MO and MG respectively. Experimental results indicated that the optimum contact time for MO removal was 120

mtinute.The removal efficiency (%) of both MO and MG increases as the contact time varies from 20 to 120 minutes before becoming constant, as shown in Figure 10. Consequently, 120 minutes was taken as the equilibrium time. At this point, the amount of dye desorbed from the adsorbent is in a state of dynamic equilibrium with the amount of dye adsorbed on the adsorbents.

The adsorption is rapid during the first few minutes of the reaction, which can be interpreted by the fact that at the start of adsorption, the number of active sites available on the adsorbent surface is much greater than the number of sites remaining after a certain time. For long contact times, the molecule needs time to diffuse into the adsorbent pore [43], while the saturation of the adsorbent surface interprets the remaining quantity not adsorbed (all adsorption sites are occupied). Therefore, the equilibration time of 120 minutes was sufficient in this case as maximum adsorption occurred during this time. It was due to the aggregation of the dye particles with increasing contact time, which made it almost impossible to diffuse deeper into the adsorbent structure at higher energy sites. This aggregation canceled out the influence of contact time as the pores filled in and began to offer resistance to diffusion of aggregated dye molecules into the adsorbents [54].

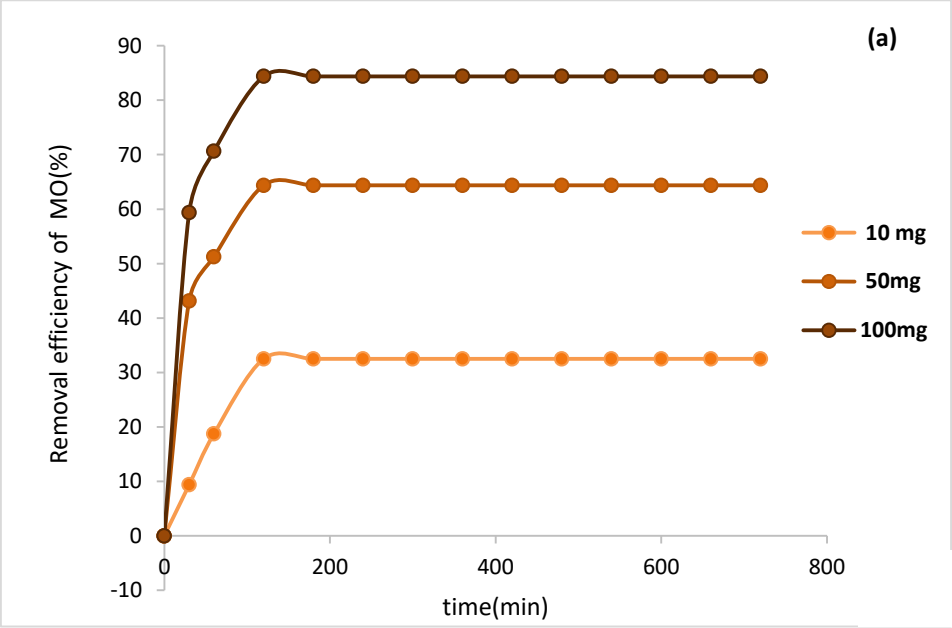

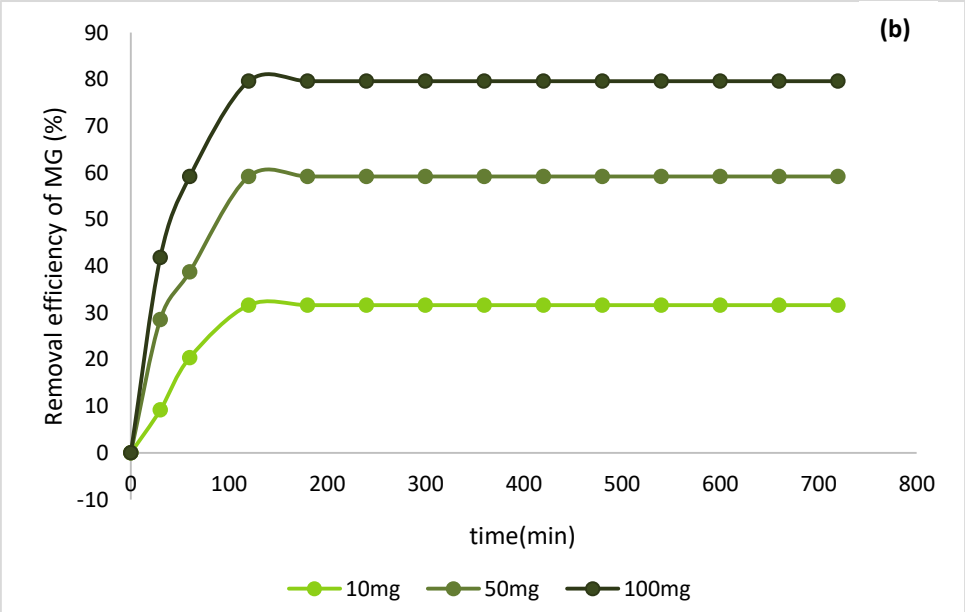

Fig.11 The effect of the contact time on the adsorption of methyl orange **(a)** and of methyl green **(b)** by $BiMgFeO_4$/activated carbon composite.

3.6.4. Influence of the temperature on the absorption of methyl orange and Methyl Green by ($BiMgFeO_4$/activated carbon) composite

The Figure below (Fig.12) displays the variation of temperature versus the removal efficiency (%) of methyl orange and Methyl Green on ($BiMgFeO_4$/activated carbon) composite

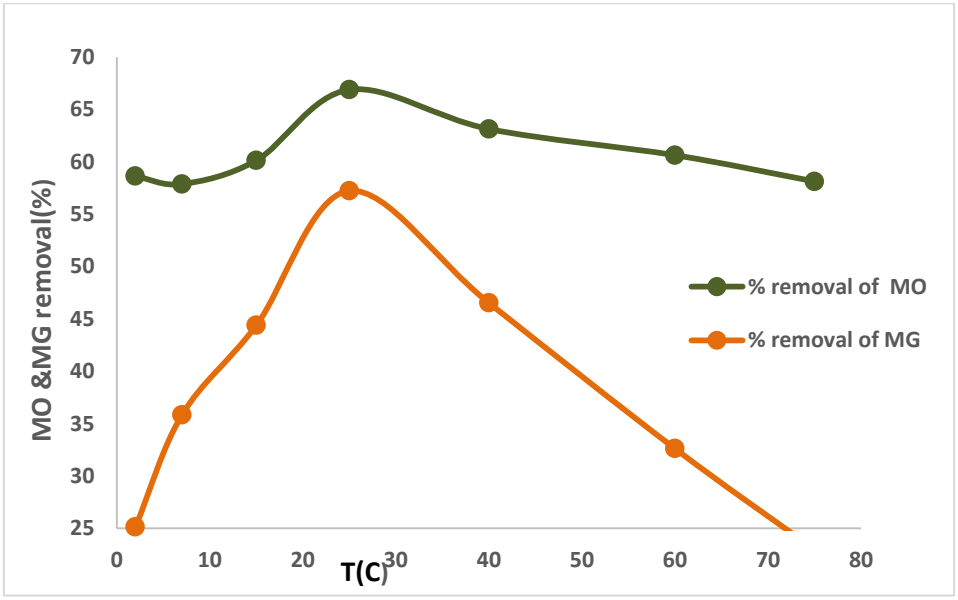

Fig. 12 Effect of temperature on MG and MO dyes adsorption on $BiMgFeO_4$/activated carbon composite. [Dye] = 50 mg. L^{-1}, adsorbent amount = 50 mg

It is known that increasing temperature increases the rate of diffusion of adsorbate molecules through the outer boundary layer and inside the adsorbent particles, due to the decrease in solution viscosity [55]. Figure 12 reveals that at 25 °C, the maximum removal rate of the MO dye on $BiMgFeO_4$/ Activated Carbon composite was 66.87%. At the same temperature, it was 81.28% for MG. This suggests that thermal excitation of the adsorption reaction is not required above 25°C to enhance the adsorption capacity of composite ($BiMgFeO_4$/Activated carbon) for methyl orange and methyle green.

From the comparison of the two curves in the figure above (Fig.12), we conclude that room temperature is the most suitable temperature for the maximum removal of the methyl orange (anionic dye) and the methyle green (cationic dye) by the composite prepared. An increase in temperature is not favorable to the adsorption phenomenon, which could prove that this is an exothermic mechanism.

3.6.5. Adsorption Kinetic

The speed at which the constituents diffuse in the adsorbent and the fluid as well as the adsorbent-adsorbate interaction determine when the thermodynamic equilibrium between the adsorbate in the liquid phase and the adsorbate fixed on the solid is reached. We can examine the impact of contact time on the dye's retention by analyzing the dye's adsorption on the nano ferrite as a function of time. For this purpose, the pseudo-first order (Eq. 5) and the pseudo-second order models have been used to explain the mechanism of the methyl orange and the methyl green adsorption kinetics on the $BiMgFeO_4$/ activated carbon composite. (Eq. 6) [56, 57]:

$$\mathbf{ln(Q_{ads} - Q_t) = ln\ Q_{ads} - K_1 t} \quad (5)$$

$$\frac{\mathbf{t}}{\mathbf{Q_t}} = \frac{\mathbf{1}}{\mathbf{Q_e^2 \times K_2}} + \frac{\mathbf{t}}{\mathbf{Q_e}} \quad (6)$$

Qe (mg/g): the equilibrium adsorption capacity,

Qt (mg/g) : the adsorption capacity at time t

k_1 (mn^{-1}) is the constant of the pseudo-first order model. And k_2 ($g.mg^{-1}.mn^{-1}$) constant of the pseudo-second order model.

For a concentration of both the methyl orange and the methyl green dyes studied equal to 50 mg/L, the values of the quantity adsorbed, the constant k_1 of the pseudo-first order model, the constant k_2 of the pseudo-second order model, as well as the correlation coefficient are well grouped in the following table (Table 2).

Dye	Pseudo-first order model				Pseudo-second order model		
	R^2	$k_1(min^{-1})$	$Q_1(mg.g^{1})$	$Q_{exp}(mg.g^{-1})$	R^2	k_2 $(g.mg^{-1}.mn^{-1})$	$Qe(mg.g^{-1})$
MO	0.95	0.0265	69.762	77.031	0.999	0.00209	78.125
MG	0.981	0.0177	59.465	62.031	0.998	0.00119	63.694

Table 2 Pseudo-first-order and pseudo-second-order models parameter

From the table above (Table 2), it can be seen that the values of the R^2 correlation coefficients are very high with the pseudo-second order model, and are all close to the unit (R^2= 0.999 for the MO and 0.998 for the MG), far exceeding those obtained with the pseudo-first-order model (respectively R^2= 0.95 and 0.981). Likewise, the equilibrium adsorbed quantities (Qe) are very close to the values found experimentally. These last two observations lead us to believe that the adsorption process of both MO and MG on the prepared composite does indeed follow the pseudo-second order model. The pseudo-first order parameters applied to the adsorption of MO and of MG on the $BiMgFeO_4$/activated carbon composite were determined by extrapolation of the curve representing the variation of Ln (Q_e-Q_t) as a function of time t (min) (Fig. 13).

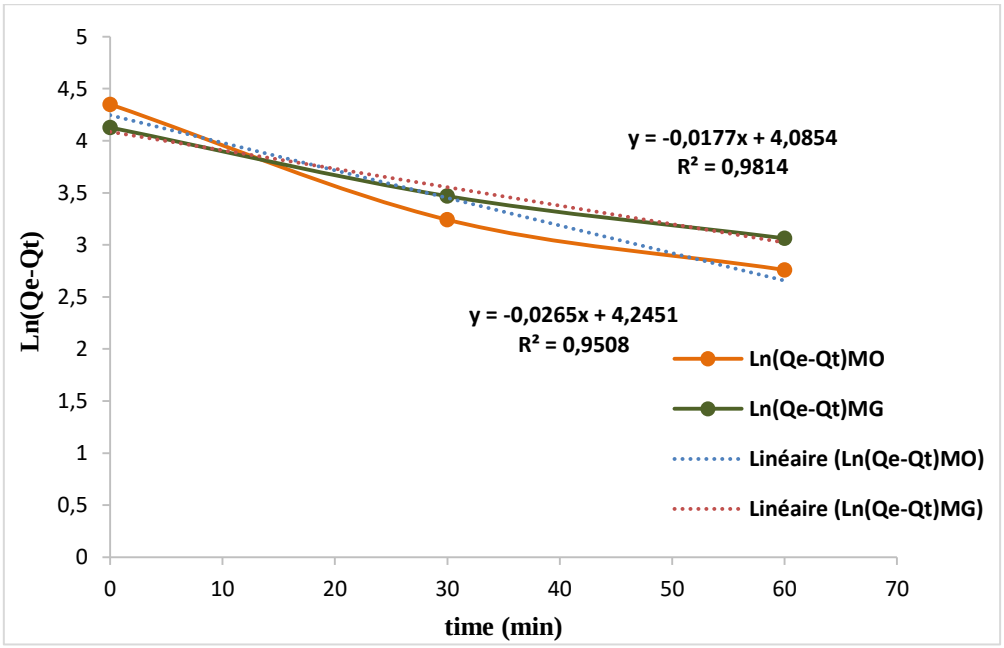

Fig.13 Pseudo-first order model applied to the adsorption of MO and of MG on the ($BiMgFeO_4$/activated carbon) composite

As can be seen from the above Figure (Fig. 13), the adsorption kinetics of methyl orange and methyl green by our composite do not follow first-order kinetic, as the experimental adsorbed amount differs from the calculated one and the correlation coefficient values are slightly different from unity. However, the figure below (Fig.14) clearly illustrates that the results of the pseudo-second order kinetic model obey the adsorption of both Methyl Orange and Methyl Green dyes onto the $BiMgFeO_4$/activated carbon composite . The two quantities, k_2 constant of the pseudo-second order model, and Qe the adsorbed capacity at equilibrium, correspond respectively to the y-intercept and the slope of the straight line representing the variation of t /Q_t as a function of time t (min), and the values of the regression coefficient are given in the Table 2 above.

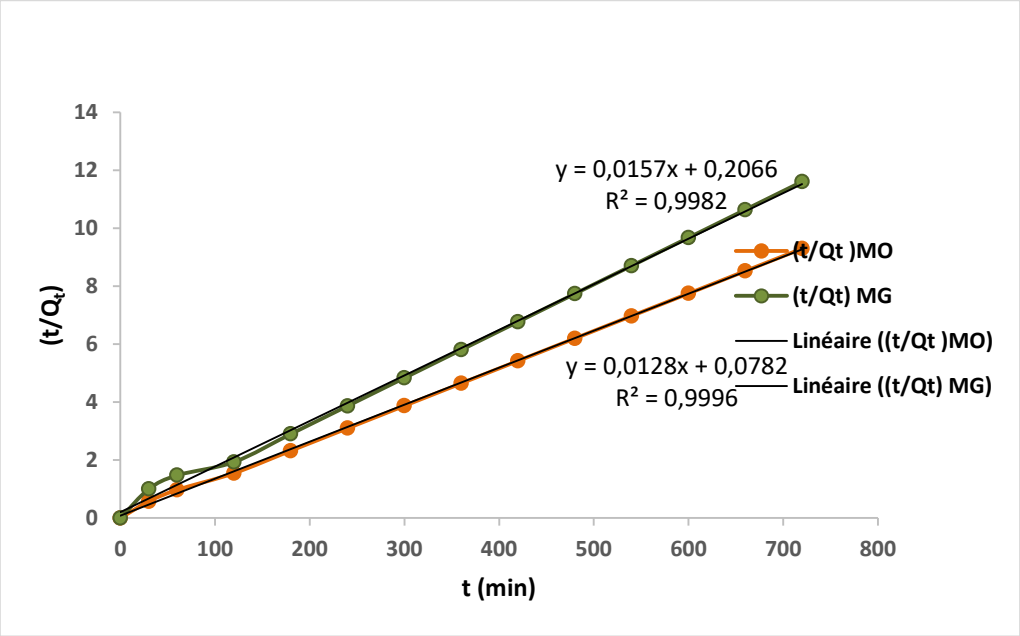

Fig. 14 Pseudo-second order model applied to the adsorption of MO and of MG on the composite.

3.6.6. Adsorption thermodynamics

The adsorption thermodynamic constants are the standard enthalpy variation (ΔH_0), the standard Gibbs free energy variation (ΔG_0), and the standard entropy variation (ΔS_0). They were calculated as following equations, Eq. (7) and Eq. (8) [58].

$$\Delta G_0 = -RT \ln K_L \quad (7)$$

$$\ln K_L = \frac{\Delta S_0}{R} - \frac{\Delta H_0}{RT} \quad (8)$$

Where T is the absolute temperature in Kelvin, K_L (L. mol^{-1}) is Langmuir's constant, R is the universal gas constant (8.314 J. $mol^{-1}K^{-1}$), and ΔH_0 and ΔS_0 are determined from the linear plot slope and the intercept of Ln K_L = f (1/T) (Fig. 15). The ΔG_0 values established by the table below (Table 3) were

negative. This proved the thermodynamically spontaneous nature of the MO and the MG adsorption. The standard free enthalpy variation values decreased with increasing temperature, supporting the exothermic nature of the adsorption process.

Dye	ΔH_0(kJ.mol $^{-1}$)	ΔS_0(J.mol^{-1} K^{-1})	ΔG_0(kJ.mol^{1})				
			275K	288K	298K	333K	348K
MO	-7.965	90.032	-29.894	-32.698	-34.782	-37.952	-39.286
MG	-3.09	83.022	-25.389	-26.654	-27.513	-30.399	-31.605

Table 3 Thermodynamic parameters for the adsorption of MO and MG on $BiMgFeO_4$/activated carbon composite

The adsorption process of Methyl Orange (MO) and Methyl Green (MG) on the $BiMgFeO_4$/activated carbon composite was exothermic, as indicated by the negative ΔH_0 values shown in Table 3. In addition, the increased degree of freedom of the adsorbed molecules and the rise in molecular disorder at the solid/liquid interface of the adsorption process was indicated by the positive values of ΔS_0. Since ΔH_0 and ΔS_0 have opposing signs, changing the temperature has no discernible effect on the free enthalpy variation's sign or value.

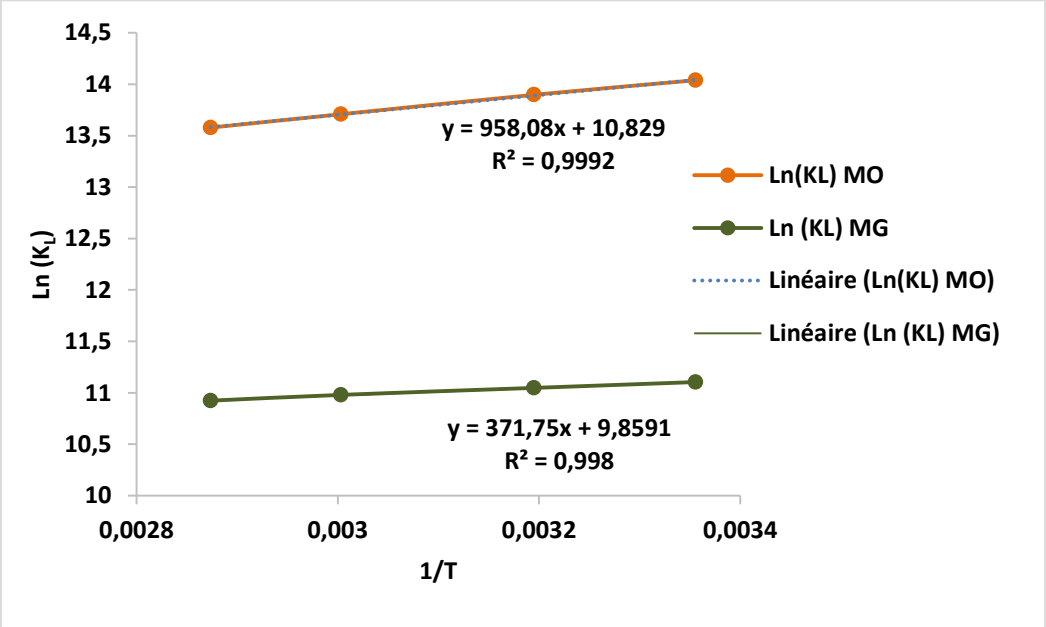

Fig. 15 Ln (K_L) versus (1/T) for MO and MG adsorption on $BiMgFeO_4$/activated carbon composite

3.6.7. Adsorption isotherm of methyl orange and methyl green on ($BiMgFeO_4$/activated carbon) composite

To assess the experimental results, models like Freundlich (Eq. 11) and Langmuir (Eq. 9) were employed. The Langmuir isotherm model is one of the isotherms that are most frequently used in adsorption to evaluate an adsorbate's highest potential for adsorption on an adsorbent. Adsorption must occur on a homogeneous adsorbent surface with monolayer coverage of adsorbate. Furthermore, according to this concept, adsorption occurs in specific homogenous, energetically similar sites [59].

$$\frac{1}{Q_e} = \frac{1}{Q_m} + \frac{1}{Q_m K_L C_e} \quad (9)$$

With K_L ($L.mg^{-1}$) is Langmuir equilibrium constant related to the affinity of adsorption, Q_m ($mg.\ g^{-1}$) is the maximum adsorption capacity in monolayer, and Ce is the concentration at equilibrium. The dimensionless equilibrium constant for the Langmuir isotherm can be expressed as (Eq. 10) [50]:

$$R_L = \frac{1}{1+K_L C_0} \quad (10)$$

The separation factor, R_L is defined by (Eq. 10) . The adsorption isotherm is unfavorable when $R_L > 1$, it is linear when $R_L = 1$, it is favorable when $0 < R_L < 1$ and it is irreversible when "R_L=0 ".
The Freundlich model assumes heterogeneous surface energy. This model is widely used to describe multilayer adsorption [60]. The no-linear form of the Freundlich can be expressed as follows:

$$\mathbf{Ln Q_e = Ln K_F + \frac{1}{n} Ln C_e} \quad (11)$$

Where $\mathbf{K_F}$ is the Freundlich constant (heterogeneity factor), and **1/n** is the Freundlich coefficient. **n** is related to sorption affinity and K_F is related to the sorption capacity.

When the coefficient **n** is between 1 and 10, the adsorbent's efficiency in adsorption is increased [61]. Actually, if **n=1**, adsorption proceeds linearly, there are no interactions between the species to be adsorbed, and the energy of the adsorption sites is uniform. In contrast, the adsorbent support's surface will change in a way that enhances the adsorption capacity if **n > 1**. Nevertheless, the adsorption becomes unfavorable and the adsorption capacity sharply drops for **n < 1** or **n << 1** [62, 63].

The table below (Table 4) displays the results of the modeling studies of the adsorption isotherms for the two models (Langmuir and Freundlich) and the correlation coefficients (R^2). And the Figure 16 depicts the adsorption isotherms for both anionic and cationic dyes.

Langmuir Isotherm parameters			Freundlish Isotherm parameters		
Dye	**MO**	**MG**	**Dye**	**MO**	**MG**
Q_m(mg.g^{-1})	196.078	192.308	**1/n**	0.6807	0.616
K_L(L.g^{-1})	0.1440	0.1884	**K_f**	24.447	30.587
R_L	0.1219	0.095	**R^2**	0.992	0.98
R^2	0.996	0.996			

Table 4 Adsorption Equilibrium parameters for Langmuir and Freundlish Isotherms of the adsorption of MO and MG on the composite

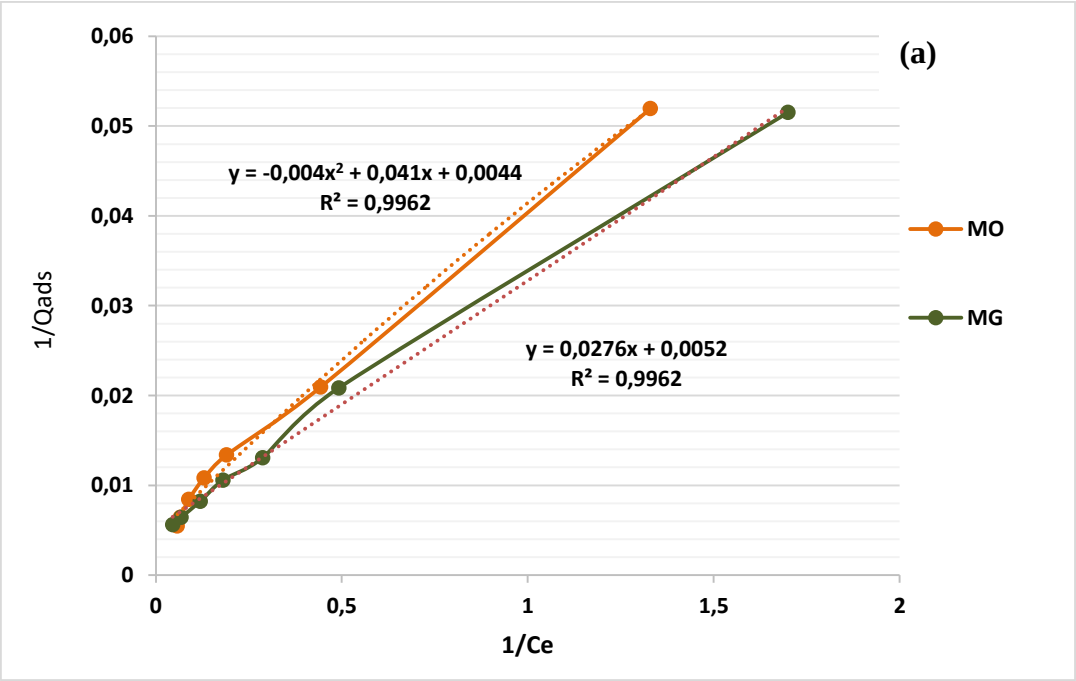

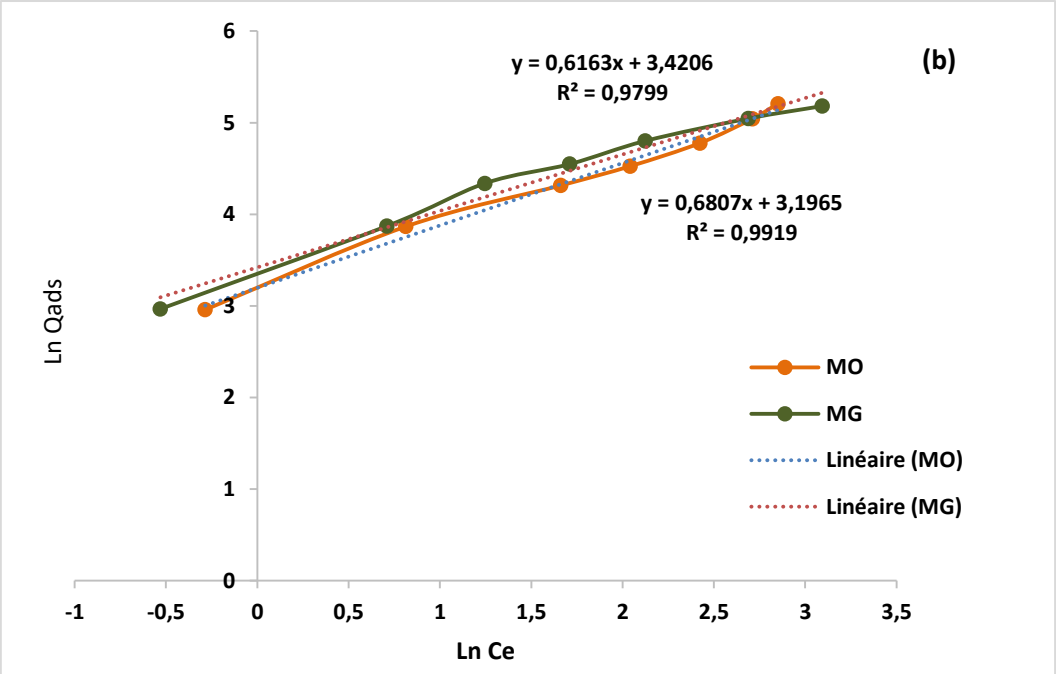

Fig. 16 Langmuir **(a)** and Freundlich **(b)** isotherms for the adsorption of MG and MO on $BiMgFeO_4$ /activated carbon

Based on the above results, we observe that the correlation coefficients for the Langmuir model (R^2= 0.996 for MG and MO) and the Freundlich model (R^2 = 0.992 for MG and 0.98 for MO) are both near to unity. We conclude that the Langmuir model best fits the experimental data. The estimated values of the separation factor "R_L" are always in an interval of 0 and 1. The results obtained confirm that the $BiMgFeO_4$/activated carbon composite has an effective MO and MG adsorption process.

3.6.7. Isosteric heat of adsorption

The isosteric heat of adsorption Qst (kJ.mol^{-1}) is the amount of heat generated when one mole of dye is absorbed by one gram of adsorbent. It was determined at constant amount of dye adsorbed (Qe = 30, 32, 34, 36, 38 mg. g^{-1}) and was calculated using the Clausius–Clapeyron equation given by the following relation where $\mathbf{\Delta H_{ads} = -Q_{st}}$ [64].

$$\frac{\boldsymbol{d(LnCe)}}{\boldsymbol{dt}} = -\frac{\boldsymbol{\Delta H_{ads}}}{\boldsymbol{RT^2}}$$

$$\mathbf{Ln}(\boldsymbol{Ce}) = \frac{\boldsymbol{\Delta H_{ads}}}{\boldsymbol{RT}} + \boldsymbol{constant}$$

The isotherm data at various temperatures were used to determine the equilibrium concentration (Ce) at constant amounts of both methyl orange and methyl green. The values of ΔH_{ads} were obtained from the slope of a plot of Ln Ce versus 1/T for different amounts of the two adsorbates (Fig.17 a,b) . The

plots of Ln Ce versus 1/T were found to be linear and the values of ΔH_{ads} were measured from the slopes of the plots.

The next table (Table 5) reports the values of the two dyes equilibrium concentration (Ce) as a function of the temperature at different values of the amount of Methyl orange and the Methyl green adsorbed at equilibrium Qe ($mg.g^{-1}$) on the prepared composite ($BiMgFeO_4$/activated carbon).

Dye	**MO**					**MG**				
Qe										
($mg.g^{-1}$)	**30**	**32**	**34**	**36**	**38**	**30**	**32**	**34**	**36**	**38**
T(K)	**Ce ($mg.g^{-1}$)**	**Ce ($mg.g^{-1}$)**	**Ce ($mg.g^{-1}$)**	**Ce ($mg.g^{-1}$)**	**Ce ($mg.g^{-1}$)**	**Ce ($mg.g^{-1}$)**	**Ce ($mg.g^{-1}$)**	**Ce ($mg.g^{-1}$)**	**Ce ($mg.g^{-1}$)**	**Ce ($mg.g^{-1}$)**
298	31.579	35.338	38.346	40.226	43.233	45.455	50.802	56.150	61.497	68.984
313	33.459	37.970	40.226	42.481	45.113	49.198	55.080	60.963	65.775	73.262
333	36.090	40.226	42.857	45.113	47.744	53.476	59.358	65.241	71.123	78.610
348	37.594	42.105	45.226	46.992	50.376	56.150	62.567	68.984	73.797	81.818

Table 5 Variation of MO and MG equilibrium concentration (Ce) as a function of the temperature at different values of the Qe on $BiMgFeO_4$/activated carbon composite

The subsequent figure (Fig.17) displays the variation of ln Ce versus 1/T for different amounts of the two adsorbates MO and MG. The slope of the resulting linear was used to calculate the values of ΔH_{ads}.

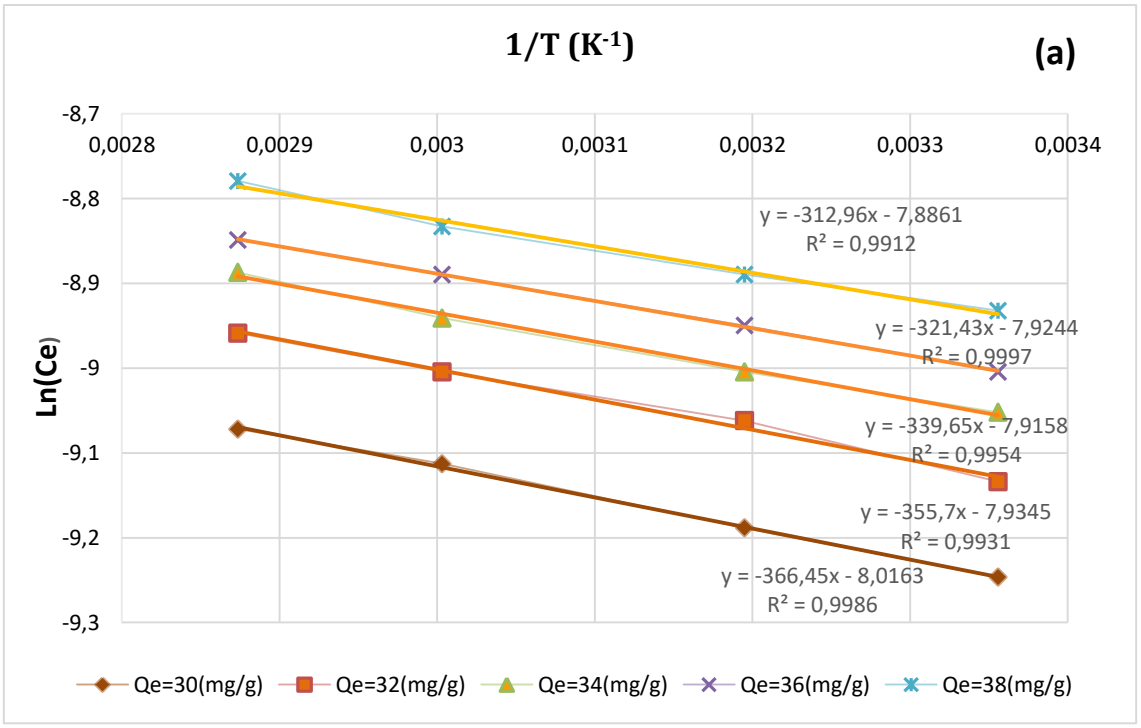

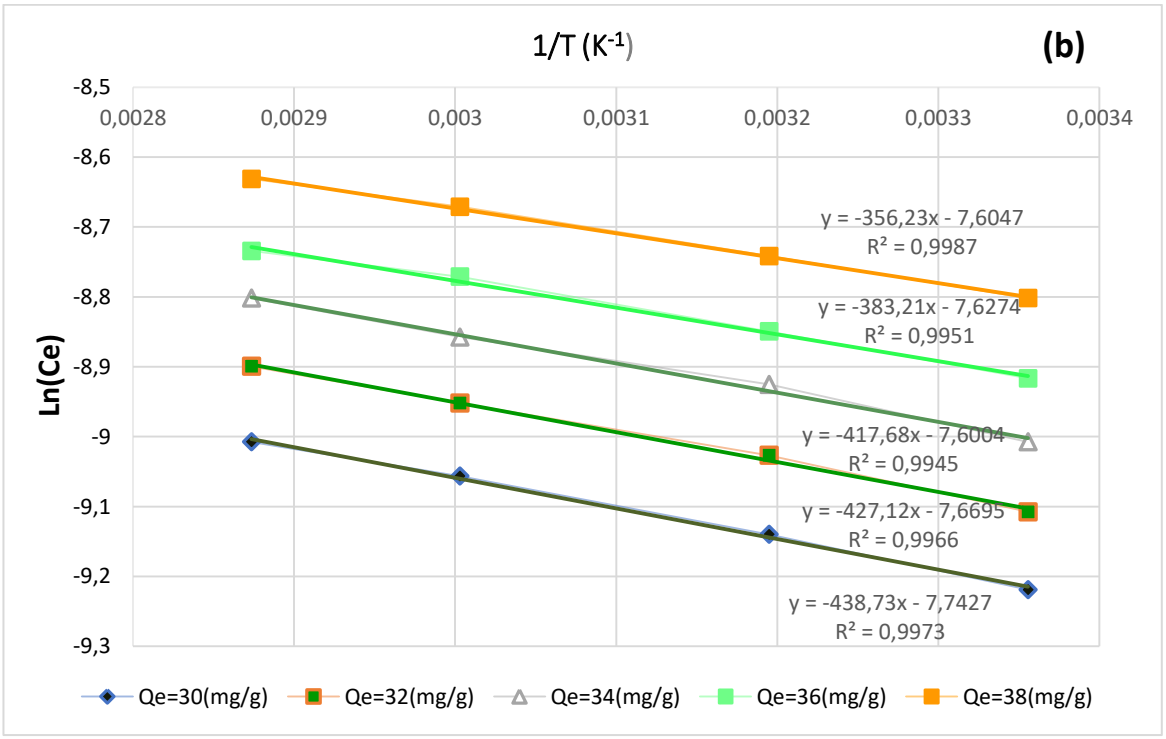

Fig.17 Plots of Ln Ce versus 1/T for adsorption onto $BiMgFeO_4$/ activated carbon composite of MO **(a),** and of MG **(b)**

The R^2 values of the isosteres and the corresponding ΔH_{ads} values are listed in the following table (Table 6) for the prepared composite as adsorbent.

Dyes	MO		MG	
Qe(mg.g^{-1})	ΔH_{ads} (KJ.mol^{-1})	R^2	ΔH_{ads} (KJ.mol^{-1})	R^2
30	-3.046	0.998	-3.647	0.997
32	-2.957	0.993	-3.551	0.996
34	-2.823	0.995	-3.472	0.994
36	-2.672	0.999	-3.186	0.995
38	-2.602	0.9912	-2.961	0.998

Table 6 Isosteric heat of adsorption of MO and MG onto $BiMgFeO_4$/activated carbon composite

The equilibrium concentration (Ce) of MO and MG at constant adsorption was obtained from isothermal data at different temperatures. As shown in Figure 17, the plot of Ln Ce versus 1/T is linear, and the ΔH_{ads}'s value was determined from the slope. The ΔH_{ads} value and R^2 for different adsorption capacities have been summarized in the table above (Table 6).

The isosteric heat of adsorption may be used to describe the surface of adsorbents. Adsorbents are homogeneous surfaces if their isosteric heat of adsorption is constant regardless of the amount of adsorbate they adsorb, and heterogeneous if it fluctuates depending on the amount of adsorbate adsorbed [65]. Adsorption capacity affected the isometric heat of adsorption when the composite ($BiMgFeO_4$/activated carbon) absorbed both dyes (MO and MG).Table 6 illustrates that ΔH_{ads} decreases as adsorption capacity increases, suggesting that the adsorbent has a heterogeneous surface. It is possible that lateral interactions between the adsorbed dye molecules, which could be followed by adsorbate-adsorbent interactions, cause the variation in ΔH_{ads} regarding the amount of the two dyes (MO and MG) on the composite [66].

The negative values for the isosteric heat of adsorption confirm the exothermic adsorption process. Furthermore, the heat of physical adsorption, which involves only relatively weak intermolecular forces such as van der Waals and electrostatic interactions, is low compared to that of chemisorption, which essentially consists of the formation of chemical bonds between adsorbate molecules and the adsorbent surface. For adsorption on adsorbents, the upper limit of Qst for physical adsorption, or physisorption, should be 80 kJ mol^{-1}. For chemical adsorption, or chemisorption, which is defined by covalent bonding, it should be between 80 and 400 kJ mol^{-1} [67]. In the present work, isosteric heat of adsorption values for methyl orange ranged from 3.046 to 2.602 kJ. mol^{-1}, and from 3.647 to 2.961 kJ.

mol^{-1} for methyl green. The above results show that the interaction between the surface of the composite ($BiMgFeO_4$/activated carbon) and the molecules of the two dyes MO and MG is a physisorption involving weak Van der Waals and electrostatic interactions.

4. Conclusion

The textile industry consumes vast quantities of water. Once discharged, they cause damage to the aquatic environment due to their stable, highly toxic, and poorly biodegradable dye loads. The main objective of the present research was to test the capacity of a new composite ($BiMgFeO_4$/activated carbon) for the adsorption of two dyes, anionic and cationic susceptible acid dyes, respectively methyl orange and methyl green, which are present in textile industry wastewater .

Whatever the pollutant, the adsorption process is an easy-to-implement method that produces very promising results for treating industrial water.

The research carried out has produced satisfactory results.The effect of factors related to operating conditions, such as contact time, adsorbent dose, pH and temperature, has been examined. The increased of the adsorbent mass led to an increase in the adsorption capacity of both dyes .

However, the percentage of MO decoloration in solution was higher, it reached 98.75 % for 150 mg of composite in 100 mL solution, while it is 94.38% for the adsorption of MG with the same dose.

In addition, acidic pH was the optimum medium for best anionic MO adsorption, while basic pH was the optimum medium for best cationic MG adsorption.

According to the kinetic analysis, the adsorption of both dyes using the composite ($BiMgFeO_4$/activated carbon) reached equilibrium after 120 minutes. Moreover, the adsorption process of both dyes could be explained by pseudo-second order kinetics.

The adsorption isotherms confirm that the adsorption process of MO and Mg on the composite was favorable. The Langmuir model is perfectly suited to the adsorption of the two dyes MO and MG on the prepared composite, with a maximum adsorption capacity of 196.078 mg/g and 192.307 mg/g, respectively, at 298 K. The **n** value of the Freundlich model is related to adsorption intensity and surface heterogeneity. The coefficient **n** (**n >1**) indicates that adsorption is favorable for both dyes.

The mesoporous structure of the composite was also shown to be advantageous for the adsorption of the MG cationic dye and the MO anionic dye. The thermodynamic parameters indicated that the adsorption of MG and MO was an exothermic process with a random distribution of dyes molecules on the adsorbent surface.

The isosteric heat of adsorption for the prepared composite ($BiMgFeO_4$/activated carbon) adsorbed both dyes (MO and MG) suggests that it is an exothermic process and that it is indeed a physisorption process characterized by low intermolecular forces between adsorbate and adsorbent. Adsorption capacity had an impact on the isosteric heat of adsorption, indicating that the adsorbent has a heterogeneous surface. The variation in ΔH_{ads} regarding the amount of dyes adsorbed on the composite may be due to lateral interactions between the adsorbed dye molecules, followed by interactions between the adsorbate and the adsorbent.

References

1. **Bhattacharya, S. Sharma & A.** (2016): *Drinking water contamination and treatment techniques.*, SpringerLink, Vol. 7, pp. 1043–1067.

2. **T.A. Aragaw, F. M. Bogale.**(2023): *Role of coagulation/flocculation as a pretreatment option to reduce colloidal/bio-colloidal fouling in tertiary filtration of textile wastewater: A review and future outlooks.*, Frontiers in Environmental Science, Vol. 11.

3. **L. Zhou, J.Yang, F. Ma, Sh. Pi, A.Tang, Ang Li.** (2021): *Recycling of Pd(0) catalysts by magnetic nanocomposites—microbial extracellular polymeric substances@Fe3O4.*, environmental management, Vol. 280.

4. **A. Larasati, Geoffrey, D. Fowlera and Nigel J. D. Grahama.(**2020) : *Chemical regeneration of granular activated carbon: preliminary evaluation of alternative regenerant solutions.*, Environmental Science: Water Research & Technology.

5. **F. M. B. Tadele Assefa Aragaw**,(2023). «Role of coagulation/flocculation as a pretreatment option to reduce colloidal/bio-colloidal fouling in tertiary filtration of textile wastewater: A review and future outlooks,» *Frontiers in Environmental Science*, vol. 11.

6. **J. Lin, W. Ye, M.Xie, D. Han Seo, J. Luo, Y.Wan.**(2023) , *Environmental impacts and remediation of dye-containing wastewater.* Nature Reviews Earth & Environment, pp. 785–803.

7. **R. Kishor, R. N. Bharagava ,G. Saxena.** (2018.) :*Industrial wastewaters: The major sources of dyes contamination in environment, ecotoxicological effects and bioremediation approaches.*

8. **Soltani, Ali, Faramarzi, Mehdi et Parsa, S. A. Mousavi.(**2021): *A review on adsorbent parameters for removal of dye products from industrial wastewater.*, Water Quality Research Journal, pp. 181–193.

9. **S.Mourdikoudis, A. Kostopoulou, A. P. LaGrow.**(2021): *Magnetic Nanoparticle Composites: Synergistic Effects and Applications.*, Advenced science .

10. **Govan, Joseph.**(2020): *Recent Advances in Magnetic Nanoparticles and Nanocomposites for the Remediation of Water Resources.*, Magnetochemistry 2020.

11. **Saad, S., Amor, S.B. & Slimane, A.B.** (2022)**.** Preparation of Magnesium Doped Magnetic Nanoferrite and its Clay-Based composite: Application to the Removal of an Anionic Dye from Wastewater. Chemistry Africa 5, 589–606. https://doi.org/10.1007/s42250-022-00343-2

12. **R. Ikram, B. Mohamed Jan , P. B. Nagy and T.Szabo.(**2023): *Recycling waste sources into nanocomposites of graphene materials: Overview from an energy-focused perspective.*, De Gruyte.

13. **C.Carlson, A. Ebben.** (2023): *A Look at Activated Carbon Thermal Regeneration.*, FEECO International .

14. **H. da Silva Santos, Y. Xiao, N. Chaukura, Josephine M. Hill, R. Selvasembian, C. L.P.Silva Zanta and L. Meilib,(**2022): *Regeneration of dye-saturated activated carbon through advanced oxidative processes: A review.*, Heliyon, Vol. 8.

15. **A. Bhatnagar , W.Hogland , M.Marques , M. Sillanpää.(**2013): *An overview of the modification methods of activated carbon for its water treatment applications.*, Chemical Engineering Journal, Vol. 219.

16. **S. Reza Ph.D, Ch. Sing Yun , Sh.Afroze,N. Radenahmad.** (2020) :*Preparation of activated carbon from biomass and its' applications in water and gas purification, a review..*, Arab Journal of Basic and Applied Sciences.

17. **K.Mohammedsaleh M Katubi, N. Salem Alsaiari ,F. Mohammed Alzahrani.** (2021): *Synthesis of Manganese Ferrite/Graphene Oxide Magnetic Nanocomposite for Pollutants Removal from Water.*, Processes 2021, Vol. 589.

18. **B.Verma , C. Balomajumder.(** 2020 Feb 8) *Magnetic magnesium ferrite-doped multi-walled carbon nanotubes: an advanced treatment of chromium-containing wastewater.*, pubmed .

19. **Belgacem, Ahmed et Ould Brahim, Insaf.** (2022) *Removal of Methyl Green Dye from Aqueous Solutions Using Activated Carbon Derived from Cryogenic Crushed Waste Tires.*, Research Article, Vol. 41, pp. 207-219.

20. **Wu KH, Ting TH, Li MC, Ho WD** (2006) Sol-gel auto-combustion synthesis of SiO2 -doped NiZn ferrite by using various fuels, 298:25–32

21. **R. Jemai, M. A. Djebbi ,S. Boubakri,H. Ben Rhaiem and A. Ben Haj Amara.(** 1 May 2023): *Effective Removal of Methyl Orange Dyes Using an Adsorbent Prepared from Porous Starch Aerogel and Organoclay.*, Colorants , pp. 209-229.

22. **Oksana V et al (** 2020): *The Formation of Perovskite during the Combustion of an Energy-Rich Glycine–Nitrate Precursor*, Materials (Basel).

23. **H.Gyulasaryan et al** (2023) : *Combustion Synthesis of Magnetic Nanomaterials for Biomedical Applications.*, nanomaterials-logo.

24. **Sh. J. Kashyap , R. Sankannavar, G.M. Madhu.** (2022) , *Iron oxide (Fe2O3) synthesized via solution-combustion technique with varying fuel-to-oxidizer ratio: FT-IR, XRD, optical and dielectric characterization.*, Materials Chemistry and Physics, Vol. 286.

25. **J. S. Piccin, G. L. Dotto and L. A. A. Pinto** *(2011), Adsorption isotherms and thermochemical data of fd&c red n° 40 binding by chitosan.*.brazil : Brazilian Journal of chimical engineering, Vol. 28.

26. **S. N. Taqui,(2023):** *Insights into isotherms, kinetics, and thermodynamics of adsorption of acid blue 113 from an aqueous solution of nutraceutical industrial fennel seed spent.*. 22665, s.l. : Scientific Reports .

27. **Ifelebuegu, Uduakobong A. Edet andAugustine** (2021), *Kinetics, Isotherms, and Thermodynamic Modeling of the Adsorption of Phosphates from Model Wastewater Using Recycled Brick Waste.*. s.l. : Processes 2020.

28. **Sultan Alam et al (2021),** *Adsorption Kinetics and Isotherm Study of Basic Red 5* ,Water, Vol. 13.

29. **Francisco J. Barba a, Predrag Putnik b, Danijela Bursać Kovačević b, Mahesha M. Poojary c d, Shahin Roohinejad e f 1, José M. Lorenzo g, Mohamed Koubaa**, *2017* Impact of conventional and non-conventional processing on prickly pear (*Opuntia* spp.) and their derived products: From preservation of beverages to valorization of by-products, Trends in Food Science & Technology, Volume 67, September 2017, Pages 260-270

30. **N.Zoghlami, I. Chrita, B. Bouamama, M. Gargouri, H. Zemni, A. Ghorbel** (2009) , *Genetic diversity in Tunisian Barbary fig as revealed by molecular tools: implications for conservation. Acta, Hortic., 811 59-66.*

31. **E. Amani, L. Marwa, B. S. Hichem, S.H. Amel, B. Ghada** *(2019), Morphological variability of prickly pear cultivars (Opuntia spp.) established in ex-situ collection in TunisiaSci. Hortic., 248 163-175.*

32. **H. Faouzi, Cah. O.-m.** *(2015), Le figuier de Barbarie (l'Opuntia ficus-indica): un produit de terroir pour le développement local? Aknari des Aït Baâmrane (Anti-Atlas occidental, Maroc), 271, 375-400.*

33. **Bhasker U, Yelasani V, . Ramana V, Musugu R** *(2015) Journal of Magnetism and Magnetic Materials Structural , electrical and magnetic characteristics of nickel substituted cobalt ferrite nanoparticles, synthesized by self combustion method. J Magn Magn Mater 374.*

34. **Newcombe G, Hayes R, Drikas M** *(1993) Granular activated carbon: Importance of surface proprieties in the adsorption of naturally occurring organics. Colloids Surfaces A 65–71.*

35. **Guo X, Wang J** (2019) *Comparison of linearization methods for modeling the Langmuir adsorption isotherm. J Mol Liq 296:111850*

36. **Freundlich H** (1899) *Über die Adsorption in Lösungen 1: 1334*

37. O.M. Hemeda, 2004,IR spectral studies of Co0.6Zn0.4MnxFe2−xO4 ferrites,Journal of Magnetism and Magnetic Materials,Volume 281, Issue 1,Pages 36-41,ISSN 0304-8853,

38. **Mulushoa, S. Y., Wegayehu, M. T., Aregai, G. T., Murali, N., Reddi, M. S., Babu, B. V., ... & Samatha, K.** *(2017). Synthesis of spinel MgFe2O4 ferrite material and studying its structural and morphological properties using solid state method. Chemical Science, 6(4), 653-661.*

39. **V. Annapu Reddy, Pathak N P and Nath R** *2012 J. Alloys Compd 543 206-212*

40. **Xian T, Yang H, Shen X, Jiang J L, Wei Z Q and Feng W J** *2009 J. Alloys Compd 480 889-892*

41. **Coates J., (***2000)Interpretation of infrared spectra, a practical approach, in:R.A, Encyclopedia of Analytical Chemistry,150, p.1081-1103.*

42. **M. OUEDRHIRI1,Jaaouan, K., El Mohtadi, F. Benismail, C., Achkari Begdouri, A.** *(2018). «Charbons actifs à partir des coques d'olives (Picholine marocaine): préparation, caractérisation et évaluation de leur capacité de dépollution des margines. Revue Marocaine des Sciences Agronomiques et Véterinaires, 6, 362-373.*

43. **Muibat Diekola Yahya, Kehinde Shola Obayomi, Mohammed Bello Abdulkadir, Yahaya Ahmed Iyaka, Adeola Grace Olugbenga** *(2020) Characterization of cobalt ferrite-supported activated carbon for removal of chromium and lead ions from tannery wastewater via adsorption equilibrium, Water Science and Engineering. https://doi.org/10.1016/ j.wse.2020.09.007.*

44. **Suba, V., Rathika, G., Ranjith Kumar, E.** *(2019) Enhanced Adsorption and Antimicrobial Activity of Fabricated Apocynaceae Leaf Waste Activated Carbon by Cobalt Ferrite Nanoparticles for Textile Effluent Treatment. J Inorg Organomet Polym 29, 550–563.*

45. **Thommes M, Cychosz KA** *(2014) Physical adsorption characterization of nanoporous materials: progress and challenges. Adsorption 20:233–250.*

46. **Sing K** *(2001) Review about The use of nitrogen adsorption for the characterization of porous materials. Colloids Surf, A 187–188:3–9.*

47. **Sing KSW, Everett DH, Haul RAW, Moscou L, Pierotti RA, Rouquerol J, Siemieniewska T (1985) Reporting physisorption data** *for gas/solid systems with with special reference to the determination of surface area and porosity. Pure App Chem 57:603–619.*

48. **Gelb LD, Gubbins KE** *(1999) Pore Size Distributions in Porous Glasses: A Computer Simulation Study, Langmuir 15(2):305–308.*

49. **Lim, C.K.; Bay, H.H.; Noeh, C.H.; Aris, A.; Majid, Z.A.; Ibrahim, Z.,** *(2013), Application of zeolite-activated carbon macrocomposite for the adsorption of Acid Orange 7: Isotherm. kinetic and thermodynamic studies. Environ. Sci. Pollut. Res. , 20, 7243–7255*

50. **Al-Degs, Y.S.; El-Barghouthi, M.I.; El-Sheikh, A.H.; Walker, G.M.,** (2008), Effect of solution pH, ionic strength, and temperature on adsorption behavior of reactive dyes on activated carbon. Dyes Pigm. 77, 16–23.

51. **A. Ahmad, S. H. M. Setapar, C. S. Chuong, A. Khatoon, W. A. Wani, R. Kumard, M.Rafatullah,** (2015) Recent advances in new generation dye removal technologies: novel search for approaches to reprocess wastewater RSC Adv., 5,30801-30818.

52. **Ahmed, Muthanna J.** *(2016) Preparation of Activated Carbons from Date (Phoenix Dactylifera L.) Palm Stones and Application for Wastewater Treatments: Review.‖ Process Safety and Environmental Protection 102: 168–82*

53. **Mahmoodi, N. M., & Maghsoodi, A.** *(2014). Kinetics and isotherm of cationic dye removal from multicomponent system using the synthesized silica nanoparticle. Desalination and Water Treatment, 54(2), 562–571*

54. **Nevine Kamal,**2008 Amin,Removal of reactive dye from aqueous solutions by adsorption onto activated carbons prepared from sugarcane bagasse pith,Desalination,Volume 223, Issues 1–3,Pages 152-161,ISSN 0011-9164

55. **Gamal A.M., S.A. Abo Farha, H.B. Sallam, G.E.A. Mahmoud.** 2010. ―Kinetic Study and Equilibrium Isotherm Analysis of Reactive Dyes Adsorption onto Cotton Fiber.‖ Nature and Sci.

[56] **Ho, Y.S.; Mckay, G**.*,1999, Pseudo-second order model for sorption processes. Process Biochem., 34, 451–465. Cinetique*

*[*57] **Revellame, E. D., Fortela, D. L., Sharp, W., Hernandez, R., & Zappi, M. E.** (2020). Adsorption kinetic modeling using pseudo-first order and pseudo-second order rate laws: A review. Cleaner Engineering and Technology, 1, 100032.

[58] **Gobi, K.; Mashitah, M.D.; Vadivelu, V.M.** Adsorptive removal of methylene blue using novel adsorbent from palm oil mill e_uent waste activated sludge: Equilibrium, thermodynamics and kinetic studies. Chem. Eng.J. 2011, 171, 1246–1252.

[59] **Mall, I.D.; Srivastava, V.C.; Agarwal, N.K**. Removal of Orange-G and Methyl Violet dyes by adsorption onto bagasse fly ash—kinetic study and equilibrium isotherm analyses. Dyes Pigment 2006, 69, 210–223.

[60] **R. Baccar, M. Sarra, J. Bouzid, M. Feki, P. Blanquez,** 2012,Removal of pharmaceutical compounds by activated carbon prepared from agricultural by-product. Chem. Eng. J. 211-212 -310-317.

[61] **Khayyun, T.S., Mseer, A.H.** Comparison of the experimental results with the Langmuir and Freundlich models for copper removal on limestone adsorbent. Appl Water Sci 9, 170 (2019).

[62] **H. Deng, G. Zhang, X. Xu, G. Tao, and J. Dai,** 2010,"Optimization of preparation of activated carbon from cotton stalk by microwave assisted phosphoric acid-chemical activation, Journal of Hazardous Materials, vol. 182, no. 1-3, pp. 217–224.

[63] **S. Gao, R. Sun, Z. Wei, H. Zhao, H. Li,**2009, and F. Hu, "Sizedependent defluoridation properties of synthetic hydroxyapatite," Journal of Fluorine Chemistry, vol. 130, no. 6, pp. 550–556.

[64] **Gupta, V.K.** (1998) Equilibrium Uptake, Sorption Dynamics, Process Development and Column Operations for the Removal of Copper and Nickel from Aqueous Solution and Wastewater Using Activated Slag, a Low-Cost Adsorbent. Industrial & Engineering Chemistry Research, 37, 192-202. https://doi.org/10.1021/ie9703898

[65] **Bae, Y.-S. and Snurr, R.Q.** (2010) Optimal Isosteric Heat of Adsorption for Hydrogen Storage and Deliver Using Metal-Organic Frameworks. Microporous and Mesoporous Materials, 132, 300-303.

[66] **Shamik Chowdhury, Rahul Mishra, Papita Saha, Praveen Kushwaha** (2011), Adsorption thermodynamics, kinetics and isosteric heat of adsorption of malachitegreen onto chemically modified rice husk, desalination 265 (2011) 159–168

[67] **M. Dogan, M. Alkan,** (2003), Removal of methyl violet from aqueous solution by perlite, J. Colloid Interface Sci. 267 32–41.